 ©2026 Uspekhi Fizicheskikh Nauk, Russian Academy of Sciences

METHODOLOGICAL NOTES

PACS numbers: 41.20.Gz, 41.20.Jb, 42.25.Fx, **75.70.–i**

Superresolution effect and resolvability criterion for the waves in anisotropic media

E.H. Lock, S.V. Gerus, A.V. Sadovnikov

DOI: https://doi.org/10.3367/UFNe.2026.03.040105

Contents

Abstract. **The possibility of solving the problem of overcoming the diffraction limit in anisotropic media is discussed. Experimentally and theoretically demonstrated the occurrence of the superresolution effect, in which a distinct shadow from a point object is observed at distances much larger than the values obtained from the Rayleigh resolvability criterion. In particular, on the example of diffraction of spin waves with wavelength λ, the possibility of a distinct shadow from a through-hole in a ferrite film with diameter $d < \lambda$ at a distance $L \gg \lambda$ has been proved. It is established that super-directional wave propagation and super-resolving shadow from the object arise in the direction of the normal to the isofrequency dependence of the wave at the inflection point. The criterion of resolvability is formulated, which makes it possible to carry out evaluation calculations for waves in anisotropic media and confirms the possibility of super-directional and superresolution effects in them.**

Keywords: diffraction, spin wave, superresolution effect, super-directional wave propagation, criterion of resolvability

E.H. Lock [1,a], **S.V. Gerus** [1,b], **A.V. Sadovnikov** [2,c]

[1] Kotelnikov Institute of Radio Engineering and Electronics, Russian Academy of Sciences, prosp. Vvedenskogo 1, 141190 Fryazino, Moscow region, Russian Federation

[2] Chernyshevskii Saratov State University, ul. Astrakhanskaya 83, 410071 Saratov, Russian Federation

E-mail: [a] edwin@fireras.su, [b] svg318@ire216.msk.su, [c] sadovnikovav@gmail.com

Received 16 April 2025, revised 28 January 2026

Uspekhi Fizicheskikh Nauk **196** (4) 403 – 421 (2026)

Translated by A.V. Sadovnikov, A.S. Ptashenko

1. Introduction

In optics, the possibility of overcoming the diffraction limit (i.e., the ability to observe objects whose dimensions are much smaller than the wavelength of light) has been a frequent subject of scientific discussion since the invention of the microscope and telescope in the 17th century. Apparently, the theory of resolving power for optical instruments, proposed by J.W. Rayleigh in 1879 on the basis of his well-known criterion, should have settled these debates. However, at the beginning of the 21st century, new studies dedicated to overcoming the diffraction limit are began. The intensification of this research was driven both by advances in fluorescence microscopy techniques (see, e.g., [1–3]) and by investigations into the properties of metamaterials [4, 5], in connection with the interest to the so-called 'Veselago superlens.' Such a lens could be realized using a medium with simultaneously negative permittivity ε and permeability μ [6] and could make it possible to overcome the diffraction limit. However, as it turned out, superresolution effects achieved with the Veselago superlens are provided by the near-field electromagnetic component, which does not propagate to large distances because of the rapid decay of its amplitude. Consequently, superresolution effects can be observed only near the lens itself at distances of the order of the wavelength.

Recently, researchers studying waves propagating in continuous anisotropic media have also joined the effort to overcome the diffraction limit. In addition to negative refraction — which can also be achieved with metamaterials — such physical effects as nonreciprocal and unidirectional propagation of waves, the appearance of two (several) reflected or refracted rays, negative reflection, absence of reflection, etc. have been discovered in these media [7].

Furthermore, based on studies of spin wave (SW) diffraction, super-directional propagation of these waves was predicted [8–10] and subsequently observed experimentally [11–13].

The first studies devoted to spin wave diffraction were published back in the 1980s [14–17]. In particular, Ref. [16] reported that if the length of the transducer exciting a surface SW is on the order of the spin wavelength, a noticeable concentration of wave energy occurs near certain directions as the wave propagates. Since, at that time, it was not possible to measure these directions with sufficient accuracy, the authors of Ref. [16] concluded that these directions corresponded to the cutoff angles[1] of the group velocity vector. Approximately 20 years later, Ref. [18] presented calculations of the response from a point source of harmonic oscillations for backward volume SWs. Based on these calculations, the authors of Ref. [18] concluded that the energy of excited magnons should focus along the normals drawn at the inflection points of the isofrequency dependence.[2] In Ref. [19],[3] the incidence of a surface SW on a hole in a ferrite film was studied, and the characteristics of secondary SWs — excited by the hole — were investigated. The authors of Ref. [19] also noted that the energy of SWs scattered by the hole becomes localized along specific directions. Slightly earlier, Ref. [8] provided an analytical solution of the two-dimensional problem devoted to the study of diffraction divergence of SW beam (wave packet) with a limited width and noncollinear mutual orientation of the wave vector $\mathbf{k}_0$ and the group velocity vector $\mathbf{V}_0$. Subsequently, Refs [8–10] demonstrated that the angular width of a diffracted beam excited by a thin linear transducer or a slit in an opaque screen depends not only on the ratio of the SW wavelength λ_0 to the exciter size D (as in isotropic media) but also on the curvature of the SW isofrequency dependence at the point corresponding to the wave vector. As a result, for the case $D \gg \lambda_0$, a formula was derived describing the angular diffraction divergence (angular width) of the beam as a function of the parameters of the incident SW, the anisotropic medium, and the exciter. Moreover, it was shown that this formula can be used to calculate the angular beam width for other types of SWs and for waves of different nature in various anisotropic media and structures [8]. It was established that the angular width of a diffracted beam in anisotropic media can be not only larger or smaller than λ_0/D but can even vanish. As it turned out, beams whose wave vector directed toward the inflection point of the wave's isofrequency dependence exhibit zero angular width. Physically, this means that super-directional wave propagation is possible in anisotropic media, wherein the beam does not broaden during propagation and maintains a constant width.

Subsequent experiments [11, 12] confirmed the predictions of the theoretical works [8–10], including the realization of super-directional propagation for both surface and backward volume spin waves in a ferrite slab. Consequently, Refs [8–12] significantly increased interest in studying diffraction phenomena in anisotropic media, since a successful overcoming the diffraction limit would make it possible to significantly improve the characteristics of a number of recently developed devices in acoustics, optics, and magnonics (see, e.g., Refs [20–26]). Thus, the publication of Refs [8–12, 18, 19] stimulated new research on narrowly directed and super-directional SW beams in various structures [27–30], including magnonic crystals [31, 32].

In the present work, we demonstrate that diffraction of waves in anisotropic media can give rise to superresolution effects — where the angular resolution from the observed shadow of an object is many times smaller than that predicted by the Rayleigh resolution criterion — and we formulate the condition under which such effects occur. In particular, using spin wave diffraction with wavelength λ as an example, we experimentally and theoretically demonstrate the formation of a distinct shadow from a point-like object (a through hole in a ferrite film) with dimensions $d \sim \lambda$ and $d \ll \lambda$ at a distance $L \gg \lambda$.

2. Fundamental relations describing spin wave propagation in a tangentially magnetized ferrite slab

The existence of spin waves in ferromagnets was first predicted theoretically by F. Bloch in 1930 [33]. Spin waves are electromagnetic in nature and represent oscillations of atomic magnetic moments that transmitte from atom to atom in magnetically ordered crystals [34]. In the 1960s–1970s, monocrystalline ferrite films — particularly yttrium iron garnet (YIG) films — began to be grown by liquid-phase epitaxy. This advancement made it possible to substantially reduce propagation losses of spin waves (SWs) in such films and led to a significant increase in both experimental and theoretical studies of SWs in these films and in various plane-parallel structures based on them.

In 1961, a theoretical study [35] devoted to the characteristics of SWs in a tangentially magnetized ferrite slab (Fig. 1a) was published. In Ref. [35], when describing SWs, it was proposed to neglect terms containing the factor ω/c in Maxwell's equations (i.e., to use the magnetostatic equations), since the SW wavenumber $k \gg k_0 \equiv \omega/c$ (where ω is the angular frequency of the SW and c is the speed of light). Using this method for SWs with wavenumbers $k_0 \ll k \ll 10^5\ \text{cm}^{-1}$ (for which exchange interaction can be neglected) the simple dispersion relation for SWs propagating in the plane of the ferrite slab was obtained [35, 36]:

$$\nu^2 k_y^2 - k_{1x}^2 - \mu^2 k_{2x}^2 - 2\mu k_{1x} k_{2x} \operatorname{cth}(k_{2x} s) = 0\,, \qquad (1)$$

where s is the thickness of slab *2* (see Fig. 1a); $k_{2x} = \sqrt{k_y^2 + k_z^2/\mu}$ and $k_{1x} = \sqrt{k_y^2 + k_z^2}$ are wavenumbers determining the SW distribution across the slab thickness and in the surrounding half-spaces *1* and *3*; k_y and k_z are components of the wave vector $\mathbf{k}$; $\mu = 1 + \omega_M \omega_H (\omega_H^2 - \omega^2)^{-1}$ and $\nu = \omega_M \omega (\omega_H^2 - \omega^2)^{-1}$ are the diagonal and off-diagonal components of the ferrite permeability tensor (see, e.g., [36]); $\omega_H = \gamma H_0$, $\omega_M = 4\pi\gamma M_0$, $\omega = 2\pi f$, f is the SW frequency, γ is the gyromagnetic ratio, $4\pi M_0$ is the saturation magnetization of the ferrite, and H_0 is the magnitude of the external tangential uniform magnetic field (Fig. 1a). Dispersion relation (1) describes a single-mode surface SW whose distribution across the ferrite thickness is described by exponential functions. However, since the quantity μ can be negative over a certain frequency range, the wavenumber k_{2x} in this range may become imaginary. In this case, the SW dispersion relation takes the form

$$\nu^2 k_y^2 - k_{1x}^2 + \mu^2 k_{2x}^2 - 2\,\mu\, k_{1x} k_{2x} \operatorname{ctg}(k_{2x} s) = 0\,, \qquad (2)$$

[1] This term is explained in Section 4.
[2] This term is explained and discussed in detail in Section 4 of Ref. [7].
[3] The results of this work are discussed in more detail in Section 6.

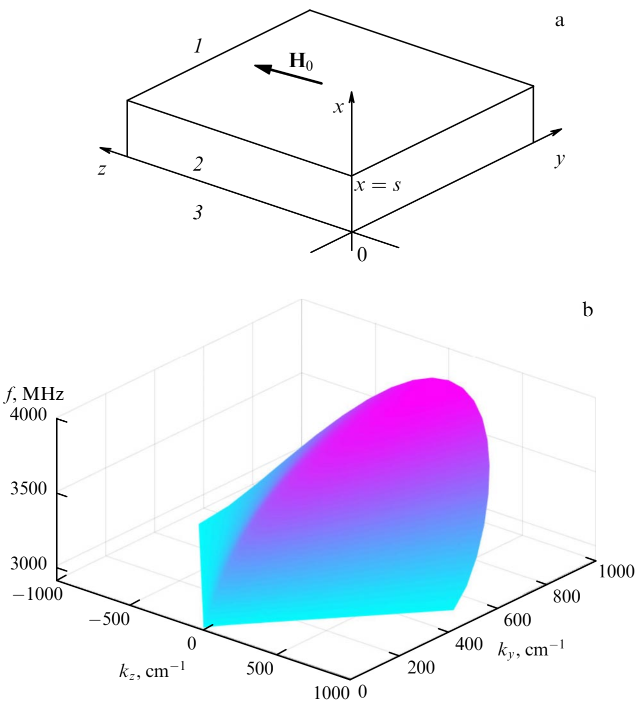

Figure 1. Tangentially magnetized ferrite slab *2* surrounded by vacuum half-spaces *1* and *3* (a) and the dispersion surface of a surface SW (b), calculated on the basis of Eqn (1) for this geometry for $H_0 = 485$ Oe, $4\pi M_0 = 1750.5$ G, and $s = 16.56$ μm for $k_y > 0$.

and describes a multimode volume SW whose distribution across the ferrite thickness is described by trigonometric functions.

Because Eqns (1) and (2) were derived within the magnetostatic approximation, the SWs described by these equations are often referred to as magnetostatic waves.[4] The dispersion surfaces and dispersion relations for surface and volume SWs in a free ferrite film are discussed in detail and presented in Ref. [35].

Since the experiments and calculations described below were performed for a surface SW in a certain ferrite film, we consider in more detail the characteristics of this wave for $H_0 = 485$ Oe in a YIG film with thickness $s = 16.56$ μm and saturation magnetization $4\pi M_0 = 1750.5$ G. The SW dispersion surface calculated from Eqn (1) for $k_y > 0$ is shown in Fig. 1b (for clarity, Fig. 1b does not display the part of the dispersion surface for $k_y < 0$, which is mirror-symmetric to the shown surface with respect to the plane passing through the f and k_z axes). As is well known [35], a surface SW exists in the frequency range $f_\perp < f < f_{\max}$, where $f_\perp = \gamma\,(H_0^2 + 4\pi M_0 H_0)^{1/2}$ and $f_{\max} = \gamma\,(H_0 + 2\pi M_0)$ are the lower and upper frequencies of the wave spectrum, respectively; for the chosen parameters, $f_\perp = 2918$ MHz and $f_{\max} = 3812$ MHz (see Fig. 1b). Below, we will present additional characteristics of the surface SW, in particular, calculated isofrequency dependencies, which represent cross-sections of the dispersion surface by planes perpendicular to the frequency axis (i.e., each isofrequency dependence corresponds to a fixed frequency value $f = \text{const}$).

[4] We note here that an exact description of SWs based on Maxwell's equations (without using the magnetostatic approximation) was recently obtained in Ref. [37]. However, below we will not use the results obtained in this work, since, firstly, for the waves studied below, the relation $k \gg k_0$ was always satisfied and, secondly, the exact dispersion equation for the surface SW is mathematically much more complex.

3. Methods for obtaining visualized patterns of spin waves: the probing method and micromagnetic simulation

In the 1980s–1990s, the spatial distribution of SW amplitude (or the wave beam profile) was measured using a probe — a small metallic loop with dimensions of ~ 0.5 mm, with was uniformly moved over the ferrite film surface along certain fixed values of one of the coordinates [14, 15, 38, 39]. Based on this measurement method, a probing method was developed in the 2010s: while the aforementioned studies measured only the SW amplitude, the Ref. [40] was the first study where a visualized pattern describing the distribution of the *complex SW amplitude* (i.e., both amplitude and phase) in the plane of the ferrite film (see below for details) was obtained. In addition to the probing method, there is another method that allows one to measure the distribution of the amplitude and phase of the SW in the plane of the studied films (or structures) — the Mandelstam–Brillouin light scattering (BLS) method (see, e.g., [41–44]). Subsequently, both methods became widely used in the study of SW, and a number of works presented visualized patterns of SW characteristics obtained using either the BLS method (see, e.g., [13, 19, 44–47]) or the probing method [11, 12, 40, 48, 49].

Briefly comparing these two methods, it should be noted that although the BLS method allows one to obtain an accuracy of the order of the optical wavelength when measuring SW distributions in the plane of ferrite films (see, e.g., [13, 19, 44–47]), this method allows one to obtain SW distribution patterns only over a small area — typically less than ~ 20 mm^2 (with an increase of the study area, the time required to carry out measurements increases significantly, which makes such experiments practically unrealistic). This limitation arises because the BLS method imposes stringent requirements on the direction and homogeneity of the magnetic field: during measurement, the sample under study (the ferrite slab) is moved, while the laser beam is focused by the lens onto the surface of the sample and remains stationary. Moreover, to obtain the SW phase distribution patterns, it is necessary to include a light phase modulator into the optical path [46, 47], which, as a rule, has a rather narrow operational frequency range, much smaller than the spectral width of the SWs under investigation.

At the same time, although the probing method has lower spatial resolution (determined by the probe aperture of ~ 0.25 mm), it enables one to measure the distribution patterns of SW in a wide frequency range over a film area of up to ~ 40 cm^2 (see, e.g., [11, 12, 48]) in a few hours, that is, to obtain diffraction patterns for SW with different frequencies simultaneously. As will become clear from the subsequent discussion, the use of this method enabled us to accomplish all intended purposes: to measure the distribution of the amplitude and phase of the SW and to obtain visualized patterns describing SW diffraction over a sufficiently large area of the ferrite film.

Because the probing method is constantly being improved to solve new experimental problems, we will briefly describe below the history of its development and specific features of its application in the studies of SW diffraction. The SW probing method evolved gradually from the 'moving transducer method,' which was employed in the 1970s–1990s to measure SW characteristics. In that approach, the receiving transducer was moved along the surface of the ferrite film either perpendicular to the wave path to measure the beam profile [14, 15, 38, 39] or along the wave path to measure the

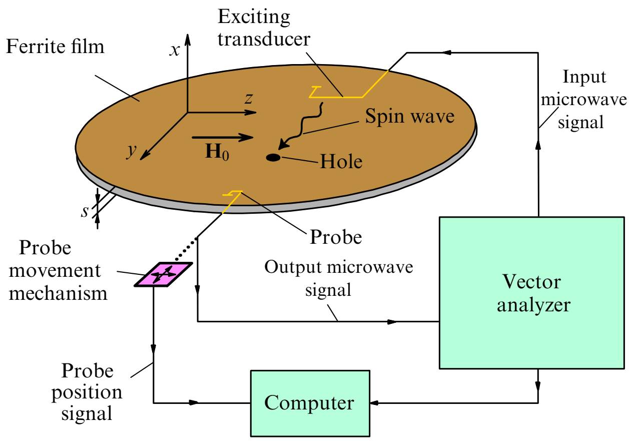

Figure 2. Scheme of experimental setup.

SW phase shift corresponding to the transducer displacement, in order to determine the wavenumber at a fixed frequency (see, e.g., [50, 51]).

Currently, in the experimental setup schematically shown in Fig. 2, the microwave probe is used as a receiving element (converting SW energy into a microwave signal). This probe is a trapezoid-shaped loop of thin, gold-plated tungsten wire. The base of the trapezoid (i.e., the distance between its grounding point and the place where it is soldered to the supply microstrip line) is ~ 0.8 mm, while the segment of the loop contacting with the film surface has an aperture of ~ 0.25 mm. Both the probe and the excitation transducer are equipped with position sensors and could rotate around an axis normal to the ferrite film plane and move over the film surface along the y and z axes by means of special mechanisms.

The pattern describing the distribution of the complex amplitude A of the microwave transmission coefficient between the transducers was measured for a fixed position of the excitation transducer. The measurements were performed as follows: for a series of y-coordinate values, the probe was continuously moved across the ferrite surface along the z-axis with simultaneous digitization of the instantaneous values of the z-coordinate and the amplitude A [40]. Since it is the SW that carries the microwave signal through the ferrite slab, then, in fact, the value *A corresponds to the complex amplitude* of the SW at the place of the film where the probe is positioned. Consequently, by processing the experimental data coming from the probe position sensors and the vector network analyzer on a computer, one can obtain normalized visualized maps of the complex amplitude A distribution at a fixed frequency over the probed region (see, e.g., the patterns presented in [11, 12]). It should be noted that because the complex amplitude A varies periodically along the film surface, the distribution pattern of its real or imaginary part corresponds quite well to the change of SW phase in the studied spatial region of the ferrite film.

In the YIG film used, which has a diameter of 76 mm, a through-hole of diameter $d = 250$ μm was fabricated using a laser (see Fig. 2). The parameters of this film, determined experimentally by the approximation of SW characteristics (this method is described in more detail in [52, 53]), are given in the previous section. The YIG film was placed in an external tangential uniform magnetic field of magnitude $H_0 = 485$ Oe. Surface SW beams were excited by a gold-plated wire linear transducer with length $D = 5$ mm and thickness 15 μm; the orientation of the excitation transducer could be fixed at various angles relative to the vector $\mathbf{H}_0$ to implement different experimental geometries. We note that with this excitation method, the transducer can be approximately considered in-phase (see §9 in [8]), and the orientations of the wave vectors of the excited SWs can be considered normal to the transducer line.

The experimental setup made it possible to obtain visualized maps of the complex amplitude A distribution for SWs simultaneously (i.e., during a single pass of the probe over the film surface) over a broad frequency range. For this purpose, a fast sawtooth frequency sweep of the vector network analyzer was performed over a frequency interval $f_{\text{begin}} < f < f_{\text{end}}$ while the probe moved comparatively slowly over the film surface (along the z-axis), such that the probe displacement during one period of the sawtooth frequency sweep was sufficiently small. Thus, as a result of the probing, the distribution of the complex amplitude $A(y, z, f)$ was measured as a function of coordinates y, z, and frequency f in the film plane; after computer processing of the data, visualized patterns describing the amplitude and phase distribution of SWs in the film plane were obtained.

We note that because SW beams can propagate over distances of tens of millimeters under certain conditions [11, 12], the experimental setup employed a magnetic system (not shown in Fig. 2) that substantially increased the spatial region with high homogeneity of the static magnetic field $\mathbf{H}_0$. Due to this system, described in detail in [54], the difference of H_0 values did not exceed 0.2% for a ferrite film surface area of ~ 50 mm in diameter.

For numerical calculations of two-dimensional SW diffraction patterns (i.e., patterns of SW amplitude distribution and averaged microwave magnetization in the ferrite film plane), a micromagnetic simulation technique was developed based on the MUMAX^3 software package, as described in detail in [45, 55]. Similar methods for calculating analogous two-dimensional patterns began to be used when modern computers and software became available in the early 21st century (see, e.g., [19, 56]). In the micromagnetic simulation method, the distribution of SW amplitude and intensity in the ferrite film plane was calculated by numerically integrating the Landau–Lifshitz equation with a dissipative term in the Gilbert form. In the calculations, the SW damping parameter was set to $\alpha = 0.005$. To avoid artifacts from waves reflected off the boundaries of the computational domain, absorbing boundary layers with a smoothly increasing damping coefficient α up to $\alpha = 1$ (corresponding to maximum dissipation) were attached to these boundaries. We also note that the elementary simulation cell area was typically set to 20 nm^2; however, when necessary — depending on calculation requirements and to optimize computation time — this value could be increased.

The developed calculation approach can be applied to study the distribution of SW amplitude and microwave magnetization inside the ferrite layer for various propagation or diffraction geometries of any SW type with arbitrary parameters. That is, the calculations can yield a two-dimensional pattern describing the propagation or diffraction of any type of SW in the plane of a ferrite film (or two-dimensional structure) at various local inhomogeneities present in that film (structure).

The selection of geometries and other parameters for which measurements and numerical calculations of diffraction patterns were performed will be discussed in the next section, in the process of calculating and analyzing SW isofrequency dependencies based on dispersion relation (1).

4. Preliminary calculations, terminology, and some information on wave propagation and diffraction in anisotropic media

First, let's discuss the terminology that will be used below.

Earlier, in Ref. [8], it was shown theoretically that the angular width of a wave beam (or ray) in anisotropic media can be not only larger or smaller than the value λ_0/D (where λ_0 is the wavelength and D is the aperture size of the exciter) — which determines the beam angular width according to the Rayleigh resolution criterion — but, under certain conditions, the angular beam width can even be zero. In fact, this means that the beam does not broaden during propagation and maintains a constant width [8]. This new unique physical phenomenon was experimentally discovered shortly thereafter in Refs [11, 12], where it was termed *super-directional wave propagation*, and the nonbroadening beams of such a wave were called as *super-directional* beams. These terms were chosen deliberately. Unlike the term super-directive antenna (see, e.g., [57], p. 244), which denotes an antenna device designed to generate a very narrow (super-directive) radiation pattern,[5] *super-directional wave propagation does not require a specially shaped radiating element*:[6] *such wave propagation in a medium that is anisotropic with respect to a given wave occurs naturally if the orientation of the beam's wave vector corresponds to the inflection point of the isofrequency dependence* (see below and Refs [8, 11, 12] for details). The super-directional wave propagation can be compared to the phenomenon of collimation created by nature itself in an anisotropic medium under certain conditions.

It should be noted that earlier, in Ref. [18], the directions of 'magnon focusing' (the authors' term) in a YIG film were theoretically found on the base of calculations of the response arising in the medium at a considerable distance from a point source of harmonic oscillations. The authors calculated that the energy of excited magnons would focus along 'caustics'[7] (the authors' term), which are parallel to the normals drawn at the inflection points of the 'slowness surface'.[8] We note, however, that in Ref. [18] the diffraction of SW was not investigated and no answers were given to the questions of what would occur if the oscillation source were not point-like, and how the width of the beam propagating in an anisotropic medium in other directions (that do not coincide with the 'caustics') will change. Answers to these questions were given a little later in Refs [8, 11, 12], where the diffraction of a finite-width SW beam was studied, and it was shown that the angular width of such a beam depends on both the wavelength and source dimensions, as well as on the spatial direction in anisotropic medium. Consequently, the studies presented in Refs [8, 11, 12] established the physical reason of 'magnon focusing' and the 'appearance of caustics' described earlier in [18, 19]: this reason is the anisotropy of the diffraction properties of the medium.

Thus, it is evident that there is a fundamental distinction between the term super-directional wave propagation and the terms listed above: for example 'focusing' implies the presence of a device that focuses the wave, and 'caustic' refers to certain reflecting (or refracting) lines (or surfaces) that sharply increase wave intensity in a particular region [58]. In contrast, super-directional wave propagation *arises due to the anisotropy of the medium with respect to the diffraction properties of the wave*, and no focusing, reflecting, or refracting devices are required for this phenomenon to occur — it is only necessary that the wave's isofrequency dependence has an inflection point (see below for details). For this reason, Refs [8, 11, 12] proposed a more adequate, physically based terminology that corresponds the essence of the observed phenomena, and which we will use below.

One may expect that, during wave diffraction in an anisotropic medium where super-directional wave propagation is possible, another unique physical phenomenon may arise under certain conditions: the superresolution effect, wherein a distinct shadow of an object is observed at much greater distances than is allowed by the Rayleigh resolution criterion. Since super-directional propagation has previously been observed for SWs [11, 12], it will apparently be possible to observe the super-resolution effect during diffraction of these waves.

To determine the frequencies and wave vectors $\mathbf{k}$ at which super-directional propagation of a surface SW occurs, the following SW characteristics were calculated for the YIG film parameters and magnetic field H_0 listed above: SW isofrequency dependences (Fig. 3); the dependence of the angle ψ, which defines the orientation of the SW group velocity vector $\mathbf{V}$, on the angle φ corresponding to the orientation of the wave vector $\mathbf{k}$ (Fig. 4a); and the dependence of the relative angular width σ[9] of the diffracted beam on the angles φ and ψ (Figs 4b and 5, respectively) for the case $D \gg \lambda$ (calculations performed in accordance with the theory of Ref. [8]).

However, before analyzing the SW characteristics shown in Figs 3–5, we briefly recall some fundamental laws concerning wave propagation and diffraction in anisotropic media.

When describing wave propagation within the framework of geometric optics, the concept of a ray is commonly used — a line along which wave energy is transferred. In anisotropic media, the ray line is always parallel to the group velocity vector $\mathbf{V}$, while the wave vector $\mathbf{k}$ may decline from the ray line at a certain angle (see, e.g., Fig. 4 in [7]). To find the ray line and the orientation of vector $\mathbf{V}$, it is necessary to draw the normal to the wave's isofrequency dependence at the point toward which the ray's wave vector $\mathbf{k}$ is directed (see, e.g., Fig. 3, as well as Figs 1 and 2 in [7]). As seen in Fig. 3, the

[5] We note here that such a device is hypothetical and practically unrealizable (see [57], p. 244).

[6] We especially notice attention of the readers to this point, as some works (see, e.g., [29]) cite Ref. [11] in the context that "antennas ensuring the formation of focused or narrowly directed wave beams" were used to excite SWs in [11]. This is not the case: in Ref. [11] there was used a conventional linear transducer that did not have focusing properties, and the narrowly directed wave beam arose in the YIG film naturally due to the super-directional propagation of the wave.

[7] For the definition and explanation of the term 'caustic,' see, e.g., p. 247 in [58] and the literature cited therein. In particular, in optics, this term refers to a phenomenon wherein light rays, upon refraction or reflection from curvilinear surfaces (water, glass), become concentrated and create bright light patterns, lines, and spots. Thus there is appeared a region of ray intersection where light intensity sharply increases (e.g., sunlight glints at the bottom of a swimming pool, patterns from light passing through a water-filled glass, rainbows, etc.). In our work, the term 'caustic,' as used in Refs [18, 19, 27–30], corresponds to the directions of super-directional wave propagation.

[8] This is the conventional term for the isofrequency dependence of acoustic waves.

[9] The definition and physical meaning of the quantity σ are explained below.

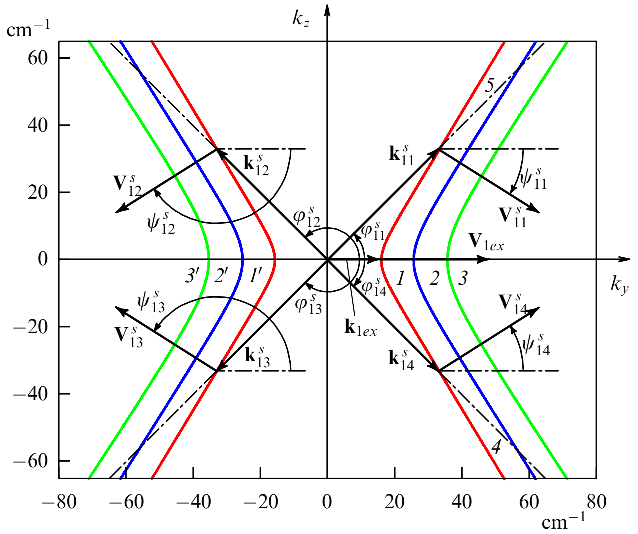

Figure 3. Isofrequency dependencies of a surface SW for frequencies 2970 (*1* and *1'*), 3000 (*2* and *2'*), and 3030 (*3* and *3'*) MHz. Curves *1–3* and *1'–3'* describe waves localized near opposite surfaces of the ferrite film. For curve *1* at frequency $f_1 = 2970$ MHz, vectors $\mathbf{k}_{11}^s$, $\mathbf{k}_{12}^s$, $\mathbf{k}_{13}^s$, $\mathbf{k}_{14}^s$ and $\mathbf{V}_{11}^s$, $\mathbf{V}_{12}^s$, $\mathbf{V}_{13}^s$, $\mathbf{V}_{14}^s$, are shown, corresponding to four super-directional beams of the surface SW, with their orientations $\varphi_{11}^s = 44.6°$, $\varphi_{12}^s = 135.4°$, $\varphi_{13}^s = -135.4°$, $\varphi_{14}^s = -44.6°$, (these angles correspond to lines *4*, *5*) and $\psi_{11}^s = -31.1°$, $\psi_{12}^s = -148.9°$, $\psi_{13}^s = 148.9°$, $\psi_{14}^s = 31.1°$, as well as the mutually collinear vectors $\mathbf{k}_{1ex}$ and $\mathbf{V}_{1ex}$ corresponding to a wave propagating along the y-axis.

surface SW is characterized by a hyperbola-like isofrequency dependence, due to which the wave vectors describing wave propagation can be oriented only within a certain angular sector (for instance, they cannot be oriented near the k_z axis in Fig. 3). The orientations φ corresponding to the boundary wave vectors (where $|\mathbf{k}| \to \infty$) are conventionally referred to as the cutoff angles of the wave vector $\mathbf{k}$, while the corresponding orientations ψ of the group velocity vector are called the cutoff angles of the group velocity vector $\mathbf{V}$ (see § 6.3 in [7] for details).

In reality, wave propagation in any medium is more complex than it seems within the framework of geometric optics: hypothetical rays correspond to wave beams that broaden during propagation due to natural diffraction divergence caused by the finite width of the initial beam. In particular, the angular beam width [10] $\Delta\psi$ for SWs (or any other wave with respect to which the medium is anisotropic) is given by the formula [11] (see § 9 in [8])

$$\Delta\psi_{\text{anis}} = \frac{\lambda_0}{D} \left| \frac{\partial\psi}{\partial\varphi} (\varphi_0) \right| , \tag{3}$$

[10] For an observer located in the far field, any wave source is a point-like, and the excited wave beams are characterized by an angular width, which is defined as the difference between the angles corresponding to a decrease of the wave amplitude to a level of 0.5 relative to its maximum value.

[11] Formula (3), corresponding to formula (32) in Ref. [8], describes the angular width of a wave beam in the far field region for the case where the exciter is in-phase or can be approximately considered as such (e.g., when SW is excited by a linear transducer). If the exciter cannot be considered in-phase, the quantity $\Delta\psi$ is determined by formula (30) in Ref. [8]. Formula (3) and formulas (30) and (32) from Ref. [8] were derived under the assumption that $D \gg \lambda_0$.

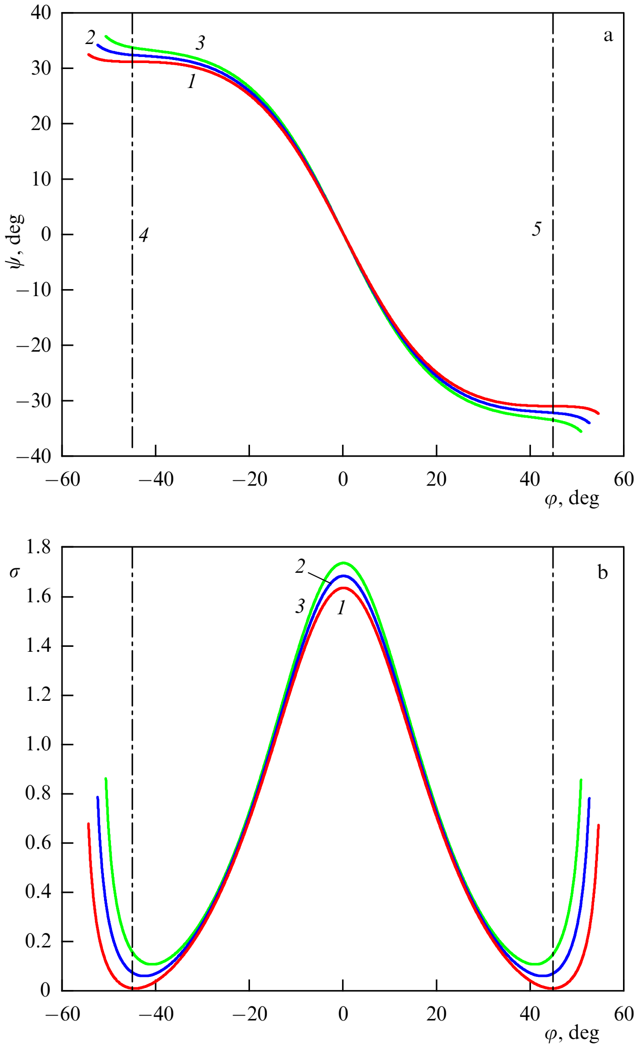

Figure 4. Dependences of the angle ψ, which determines the orientation of the group velocity vector $\mathbf{V}$, on the angle φ corresponding the orientation of the wave vector $\mathbf{k}$ (a), and dependences of the relative angular width σ of a diffracted beam on the angle φ (b) for frequencies 2970 (*1*), 3000 (*2*), and 3030 (*3*) MHz (corresponding to curves *1–3* in Fig. 3). Lines $\varphi_{14}^s = -44.6°$ (*4*) and $\varphi_{11}^s = 44.6°$ (*5*) are shown.

where D is the length of the exciter (in particular, the length of the linear transducer exciting the SW), λ_0 is the wavelength of the excited wave, and $\partial\psi/\partial\varphi\,(\varphi_0)$ is the curvature of the isofrequency dependence at the point corresponding to the wave vector oriented at angle φ_0. In isotropic media, where the wave's isofrequency dependence is a circle and the wave vector $\mathbf{k}$ and the corresponding group velocity vector $\mathbf{V}$ (normal to the circle) are always collinear, the dependence $\psi(\varphi)$ takes the form [12] $\psi = \varphi$, and consequently, the equality $\partial\psi/\partial\varphi \equiv 1$ is always true. Thus, for isotropic media, expression (3) turns into the well-known formula

$$\Delta\psi_{\text{isotr}} = \frac{\lambda_0}{D} , \tag{4}$$

which corresponds to the Rayleigh resolution criterion and is commonly used to estimate the angular width of a beam (of light or any other wave) in isotropic media (see, e.g., [59]).

[12] The dependences $\psi(\varphi)$ for a surface SW and for other waves in various anisotropic media have a more complex form (see Figs 2 and 3a in [7]).

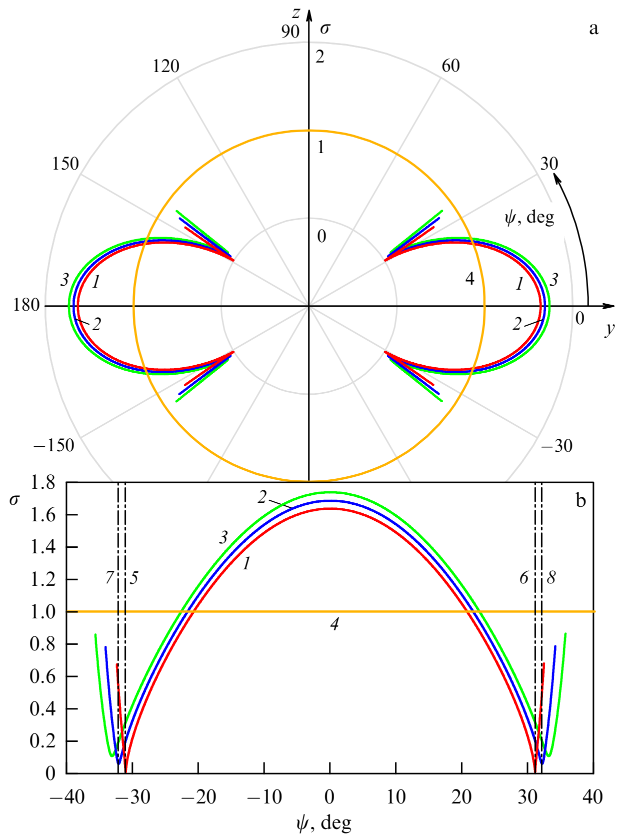

Figure 5. Dependences of the relative angular beam width σ on the angle ψ in polar (a) and Cartesian (b) coordinate systems for SWs at frequencies 2970 (*1*), 3000 (*2*), and 3030 (*3*) MHz (corresponding to curves *1*–*3* in Fig. 3) and for waves in isotropic media (*4*), for which $\sigma(\psi) \equiv 1$ (in Fig. 5b, the $\sigma(\varphi)$ dependences are shown only for the angular range $-40° < \psi < 40°$); lines *5*–*8* correspond to angles $\psi^s_{14} = -31.1°$, $\psi^s_{11} = 31.1°$, $\psi^s_{24} = -32.1°$, $\psi^s_{21} = 32.1°$; dependences *1*–*3* are finished at angles ψ equal to the cutoff angles.

Comparing formulas (3) and (4), it is evident that, unlike in an isotropic medium, the angular beam width $\Delta\psi_{\text{anis}}$ in an anisotropic medium depends on the direction of wave propagation (i.e., on the orientation φ_0 of the wave vector). The degree of diffraction divergence of a given beam in an anisotropic medium is conveniently characterized by the quantity σ, defined as

$$\sigma = \frac{\Delta\psi_{\text{anis}}}{\Delta\psi_{\text{isotr}}} = \frac{\Delta\psi_{\text{anis}}}{\lambda_0/D} = \left|\frac{\partial\psi}{\partial\varphi}(\varphi_0)\right|. \tag{5}$$

Physically, the value σ can be called the relative angular width of the diffracted beam. The value σ shows how many times the angular width $\Delta\psi_{\text{anis}}$ of a beam in an anisotropic medium is greater or less than the width $\Delta\psi_{\text{isotr}}$ of a similar beam (with the same λ_0/D ratio) in an isotropic medium. As can be seen, σ depends on the curvature of the wave's isofrequency dependence (at the point to which the wave vector is directed). Since for isotropic media the equality $\partial\psi/\partial\varphi \equiv 1$ is always true, it follows from (5) that $\sigma_{\text{isotr}} \equiv 1$ for such media (see Fig. 5). Therefore, in order to estimate the degree of diffraction divergence of a beam in an anisotropic medium, one should compare the calculated value σ with unity: when σ turns out to be smaller (greater) than unity, this signifies that beam's diffraction divergence is smaller (greater) than in isotropic media (Fig. 5).

According to formula (5), a situation may arise in anisotropic media where $\sigma = 0$, i.e., when the orientation φ of the beam's wave vector corresponds to an inflection point of the isofrequency dependence, at which $\partial\psi/\partial\varphi = 0$ (and consequently $\Delta\psi_{\text{anis}} = \sigma = 0$). In this case, super-directional beam propagation occurs in the anisotropic medium: the beam does not broaden because its angular width $\Delta\psi_{\text{anis}}$ is zero, and its absolute width remains constant during propagation. As can be seen in Figs 3–5, for a surface SW the super-directional beam can arise[13] at frequency $f = 2970$ MHz, for which $\sigma = \partial\psi/\partial\varphi = 0$ at certain angles φ and ψ (these angles are marked by dashed lines in Figs 4 and 5).

We note here that in the case of *non-in-phase* beam excitation (i.e., when a phase shift exists along the exciter), the quantity σ defined by formula (5) as the ratio $\Delta\psi_{\text{anis}}$ and λ_0/D will depend not only on the derivative $\partial\psi/\partial\varphi$, because in this case $\Delta\psi_{\text{anis}}$ is determined by formula (30) from Ref. [8]. In such a case, if $\partial\psi/\partial\varphi = 0$, then $\Delta\psi_{\text{anis}} = \sigma = 0$; however, if $\partial\psi/\partial\varphi \neq 0$, the values of σ and $\partial\psi/\partial\varphi$ will not be equal. Since the present work does not consider cases of non-in-phase exciters, below we will treat σ and $|\partial\psi/\partial\varphi|$ to be equal in accordance with formula (5).

Thus, as evident from Figs 3–5, the surface SW exhibits anisotropic properties: all wave characteristics (wavelength, angle between the energy propagation direction and the wave vector, degree of beam diffraction divergence, etc.) depend on the propagation direction, because the ferrite film placed in an external tangential uniform magnetic field constitutes an anisotropic medium with respect to this wave.

5. Geometry of incidence of a surface spin wave with large diffraction divergence on a hole in a ferrite film

Obviously, the first step is to carry out the simplest possible experiment, in which the wave incident on the hole would have a collinear orientation of the wave vector $\mathbf{k}$ and the group velocity vector $\mathbf{V}$, that is, it would be the same wave that is characteristic for isotropic media. Despite the apparent simplicity of this experiment, it may exhibit diffraction phenomena that are not typical for isotropic media, since the parameters of the diffraction beams of the SW will depend on the direction of their propagation.

To implement the described experiment, the excitation transducer was oriented parallel to the external magnetic field vector $\mathbf{H}_0$ (see Fig. 2) and positioned at a distance of 6.3 mm from the center of the hole.

As a result of processing the experimental data obtained by the probing method, a series of visualized patterns was obtained, describing the diffraction of a surface SW on the hole over the frequency range 2970 MHz $< f <$ 3100 MHz with a step of 5 MHz. One of the obtained patterns, describing the distribution of the modulus and the real part of the complex amplitude A of a surface SW at frequency

[13] For the frequency range $f_\perp < f \lesssim 2965$ MHz, the dependences $\psi(\varphi)$ lie below curve *1* and possess two extrema — a minimum and a maximum — due to which the inverse dependence $\varphi(\psi)$ becomes ambiguous over a certain angular interval of ψ. Consequently, in each direction ψ within this angular interval, beats of two interfering waves with different wavenumbers are observed. Thus, in the specified frequency range, a spatially inhomogeneous diffraction pattern arises, significantly complicating measurements (this phenomenon is described in more detail in §7 of Ref. [8]).

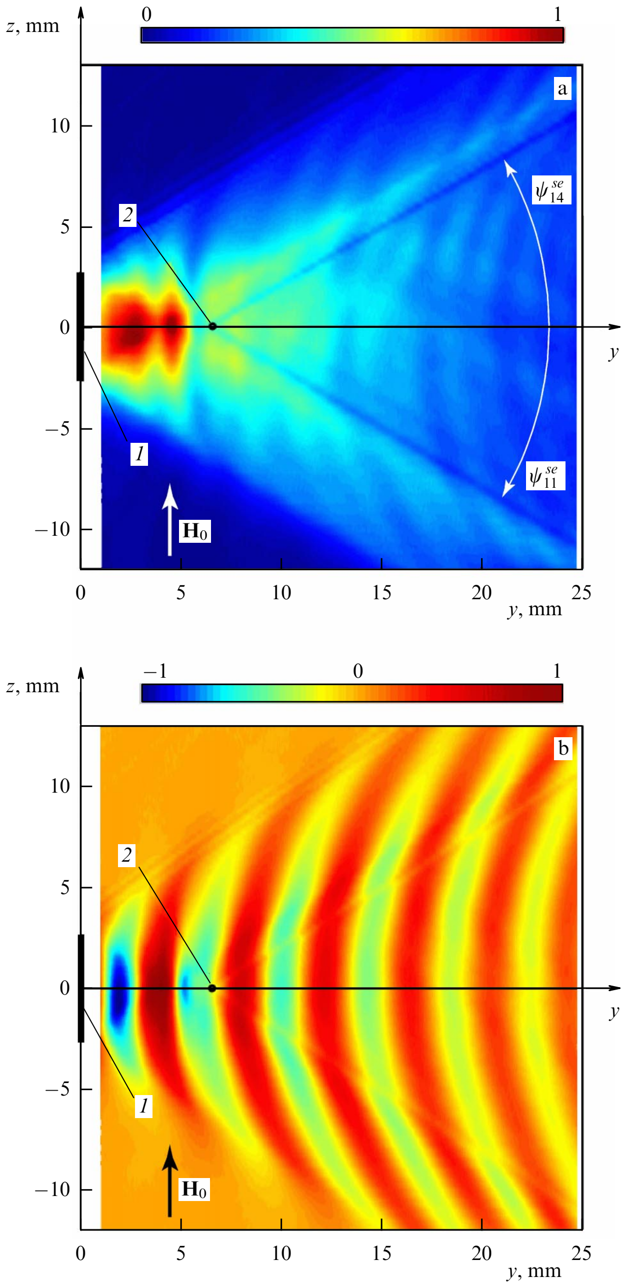

Figure 6. Experimental normalized distributions of the modulus $|A|$ (a) and the real part R (b) of the complex amplitude A of a surface SW at frequency $f_1 = 2970$ MHz during its diffraction on a through-hole *2* of diameter $d = 250$ μm in a YIG film, for the case of SW excitation by a linear transducer *1* parallel to vector $\mathbf{H}_0$.

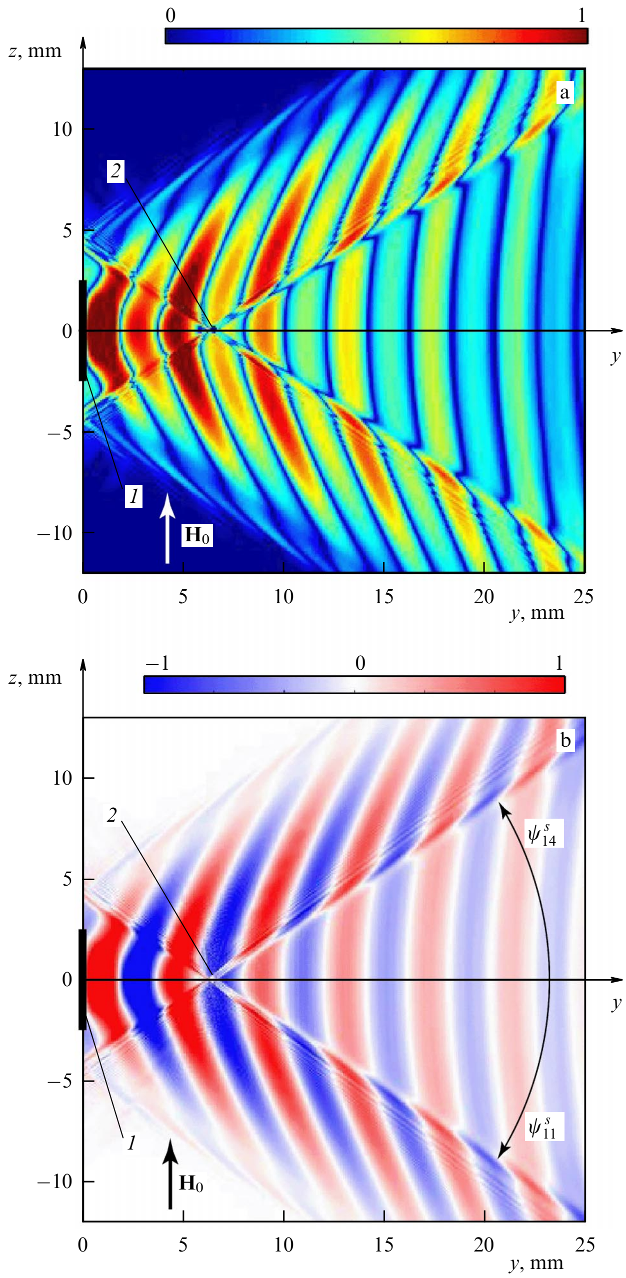

Figure 7. Calculated normalized distributions of the amplitude (a) and microwave magnetization (b) of a surface SW at frequency $f_1 = 2970$ MHz during its diffraction on a through-hole *2* of diameter $d = 250$ μm in a YIG film, for the case of SW excitation by a linear transducer *1* parallel to vector $\mathbf{H}_0$.

$f_1 = 2970$ MHz in the plane of the ferrite film, is presented in Figs 6a and 6b, respectively.

The corresponding visualized SW distributions obtained via the micromagnetic simulation technique are shown in Fig. 7. It should be noted that the calculations presented in Fig. 7b represent the distribution of the microwave magnetization of the SW, averaged over the film thickness. Since this magnetization changes direction every half-wavelength, the pattern shown in Fig. 7b effectively corresponds to the experimental distribution of the real part of the complex amplitude A displayed in Fig. 6b; moreover, both figures — 6b and 7b — quite accurately describe the SW phase distribution in the studied region of the YIG film.

As can be seen in Figs 6 and 7, the calculated and experimental diffraction patterns show good agreement.

Now, based on the above-described laws of wave propagation and diffraction in anisotropic media, we analyze the SW diffraction patterns presented in Figs 6 and 7 and consider in more detail how the excitation, propagation, and diffraction of an SW wave beam at frequency $f_1 = 2970$ MHz occurs.

Obviously, the patterns shown in Figs 6 and 7 can be regarded as the interference of two diffraction patterns: one arising from the excitation and diffraction of a finite-width wave beam during its propagation, and the other resulting from wave diffraction on the hole. We first consider the diffraction features associated with the first of the mentioned patterns.

The main portion of the microwave energy delivered to the transducer is expended on exciting waves with wave vectors $\mathbf{k}$ oriented close to the vector $\mathbf{k}_{1ex} = 15.66\ \mathrm{cm}^{-1}$ in Fig. 3 (the angles φ that determine the orientation of these vectors are close to zero[14]). Since at $\varphi \sim 0$ the quantity σ, which determines diffraction divergence, attains its maximum values (see Fig. 4b), and since the SW wavelength $\lambda(\varphi \sim 0) \sim 4$ mm is comparable to the transducer length $D = 5$ mm, the SW amplitude along the y-axis noticeably decreases with increasing y (Figs 6a and 7a). If in Figs 6 and 7 we would draw straight lines from the left and right ends of the transducer at angles equal to the group velocity cutoff angles $\psi_{1\mathrm{cut}1} = -34.3°$ and $\psi_{1\mathrm{cut}4} = 34.3°$, the region of the film within which all the SW energy is distributed will be confined between these lines.

It should be noted that for the given parameters $4\pi M_0$, H_0, and f, super-directional SW propagation can arise in the film along the $\psi^s_{11} = -31.1°$, $\psi^s_{12} = -148.9°$, $\psi^s_{13} = 148.9°$, $\psi^s_{14} = 31.1°$, corresponding to orientations of vector $\mathbf{k}$ at angles $\varphi^s_{11} = 44.6°$, $\varphi^s_{12} = 135.4°$, $\varphi^s_{13} = -135.4°$, $\varphi^s_{14} = -44.6°$, because at these angles φ and ψ the isofrequency dependence possesses inflection points, and in accordance with formulas (3) and (5) the relations $\partial\psi/\partial\varphi = 0$, $\Delta\psi = 0$ and $\sigma = 0$ take place (see Fig. 3, which shows vectors $\mathbf{k}^s_{11}$, $\mathbf{k}^s_{12}$, $\mathbf{k}^s_{13}$, $\mathbf{k}^s_{14}$ and $\mathbf{V}^s_{11}$, $\mathbf{V}^s_{12}$, $\mathbf{V}^s_{13}$, $\mathbf{V}^s_{14}$, with their orientations). This fact substantially influences the propagation of the excited SW beam: due to the absence of diffraction divergence, a significant portion of the beam energy is localized along the directions ψ^s_{11} and ψ^s_{14} drawing from the transducer center (see Fig. 6a). We note that in earlier works [14–17] devoted to SW diffraction for the case $\lambda \sim D$, it was believed that SW energy localizes near the cutoff angles of vector $\mathbf{V}$ (although in reality it localizes along directions where $\partial\psi/\partial\varphi = 0$).

We now consider the features of SW beam diffraction on an hole in the ferrite slab. As seen in Fig. 6a, a shadow from the hole is practically absent both along the y-axis and in directions lying within the angular sector $-20° < \psi < 20°$, the center of which coincides with the center of the hole. This is because in these directions $\sigma \geqslant 1$ (see Fig. 5), i.e., the diffraction divergence of the SW is large; moreover, the hole diameter $d = 250$ μm is 16 times smaller than the SW wavelength $\lambda \sim 4$ mm.

However, at $\psi \sim \psi^s_{11} = -31.1°$ and $\psi \sim \psi^s_{14} = 31.1°$ the situation changes, since *at these angles* $\sigma \sim 0$ (Fig. 5), which implies the *absence* of diffraction divergence of the wave beam. Consequently, behind the hole, in the directions[15] ψ^s_{11} and ψ^s_{14}, two distinct shadows are observed in the diffraction pattern, resembling straight 'grooves' beginning from the hole (see Figs 6 and 7), whose width equals the hole diameter d and does not change during beam propagation due to the *absence* of diffraction divergence (in Fig. 6a, the extent of these 'grooves' exceeds 20 mm)!

Summarizing the above facts, we can state the following: as a result of surface SW diffraction on an hole of diameter $d = 250$ μm, in the directions $\psi^s_{11} = -31.1°$ and $\psi^s_{14} = 31.1°$ — which correspond to a wavenumber $k^s_{11} = k^s_{14} = 45.4\ \mathrm{cm}^{-1}$ and wavelength $\lambda = 1385$ μm — a distinct shadow of width d is observed behind the aperture at a distance of $\sim L = 21$ mm. It should be noted that the wavelength $\lambda = 1385$ μm and the distance L exceed the hole diameter by $\lambda/d = 5.54$ times and $L/d = 84$ times, respectively. Estimates based on the Rayleigh resolution criterion

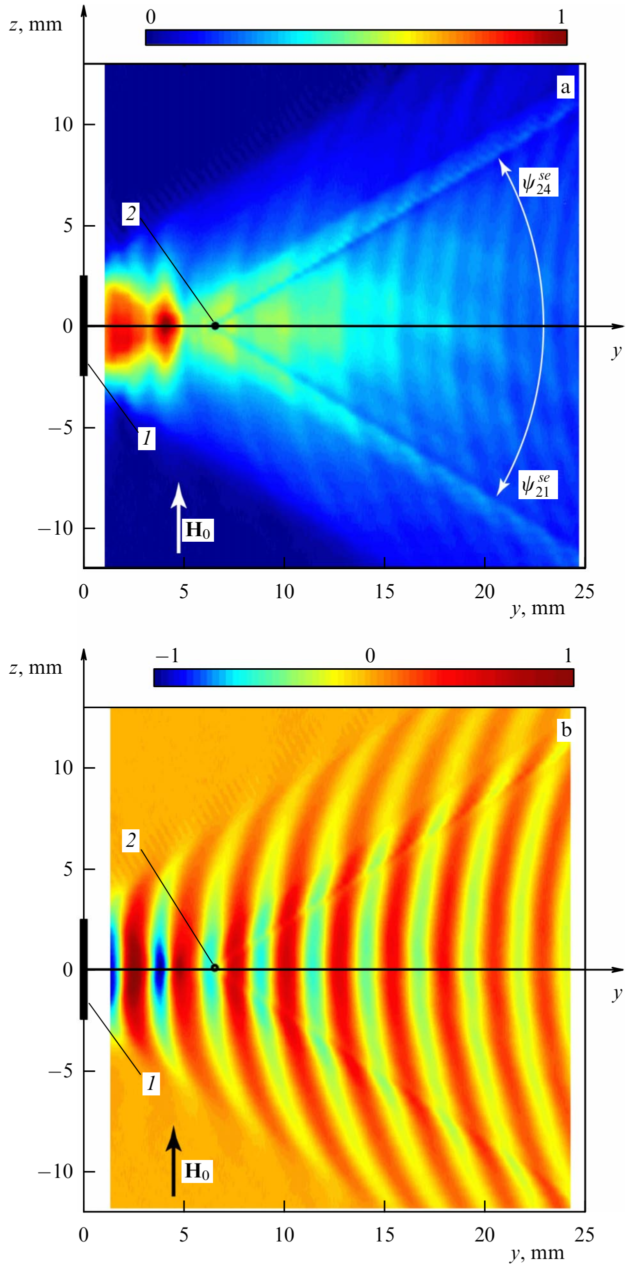

Figure 8. Experimental normalized distributions of the modulus $|A|$ (a) and the real part R (b) of the complex amplitude A of a surface SW at frequency $f_2 = 3000$ MHz during its diffraction on a through-hole *2* of diameter $d = 250$ μm in a YIG film, for the case of SW excitation by a linear transducer *1* parallel to vector $\mathbf{H}_0$.

[14] In the description of surface SWs, the angles φ and ψ, which define the orientations of vectors $\mathbf{k}$ and $\mathbf{V}$, are conventionally measured from the y-axis or the k_y-axis (see Figs 3–5), with the counterclockwise direction considered as the positive for angle measurement.

[15] For the sake of brevity, when describing the phenomena under study, we will not yet make a distinction between calculated and measured quantities. That is, we will not distinguish, for example, between the calculated direction ψ^s_{11} and the corresponding experimentally measured direction ψ^{se}_{11}, referring to both in the text as ψ^s_{11}, since the calculations and experiments show good qualitative and quantitative agreement. The differences between the measured and calculated quantities and the reasons for these differences, will be discussed in Section 9.

for isotropic media indicate that, for this geometry, a shadow from this object should not be observable.

We note that for SWs with frequencies in the range 2970 MHz $\leqslant f \leqslant$ 3030 MHz, the shadow from the hole in the diffraction patterns was also sufficiently distinct and extended (see, e.g., Fig. 8), since at these frequencies the minimum value attained by σ is less than 0.1 (see Figs 4b and 5).

However, with increasing SW frequency for $f >$ 3030 MHz, the shadow from the hole in the diffraction patterns became less distinct and exhibited stronger broadening, because as the SW frequency increases, the minimum value of σ in the dependences $\sigma(\varphi)$ and $\sigma(\psi)$ also increases, gradually approaching unity.

We also note that recently, in a study of diffraction on an hole for a backward SW excited by a transducer perpendicular to vector $\mathbf{H}_0$ [48], a shadow from the hole was also observed in the direction of super-directional wave propagation; however, the shadow was not very distinct and was observed over a shorter distance $L \sim 11$ mm.

6. Geometry of incidence of a super-directional surface spin wave beam on an hole in a ferrite film

Analyzing the visualized patterns described in the previous section, it is easy to notice that immediately after SW excitation, most of its energy spreads over a large area of the ferrite film without reaching the hole; consequently, the amplitude of the wave forming the straight 'groove'-like shadows behind the hole is relatively small. Obviously, one can propose a geometry in which practically all the energy of the excited wave reaches the hole and participates in forming the shadow behind it. In particular, it can be expected that when a super-directional beam is incident on the hole, the superresolution effect will be observed much more distinctly and at a greater distance from the hole, since in this case practically all the wave energy will be localized along the beam line. Below, we describe experiments and calculations performed for the geometry of a super-directional SW beam incident on an hole.

As calculations show (see Figs 3–5), for the given YIG film parameters, field H_0, and SW frequency $f_1 = 2970$ MHz, super-directional propagation arises when the wave vector $\mathbf{k}$ is oriented at angles $\varphi^s_{11} = 44.53°$ and $\varphi^s_{11} = -44.53°$. Therefore, the excitation transducer must be positioned on the film surface by such means (Fig. 9) to provide equality between the angle φ_{ex} corresponding the transducer line orientation relative to the vector $\mathbf{H}_0$ and the value φ^s_{11}. Obviously, before performing the experiment, it is necessary to know with what accuracy φ_{ex} must be equal to the angle φ^s_{11}? And with what accuracy should the SW frequency be chosen equal to 2970 MHz in the experiment?

To answer these questions, we discuss the features of SW propagation in the directions of super-directional propagation and in close directions on the basis of the results previously obtained in Refs [8, 11–13].

As it is seen in Fig. 4a, in the angular range $41° < \varphi < 47°$, the dependence $\psi(\varphi)$ for frequency $f_1 = 2970$ MHz (curve *1*) is practically horizontal, causing ψ to vary in the range $-31.08° < \psi \leqslant 31.01°$, i.e., changing by only hundredths of a degree relative to the direction of super-directional SW propagation $\psi^s_{11} = -31.056°$ (which corresponds to the minimum value $\sigma^s \sim 0$). As noted in the previous section, since SW energy localizes near the direction of super-directional SW propagation, *for any* (!) *orientation* φ_{ex} of the excitation transducer within the range $41° < \varphi_{ex} < 47°$, practically all the SW energy will be localized along the direction $\psi^s_{11} = -31.056°$, and the SW parameters will differ only slightly from those of a super-directional SW beam. Thus, if we excite SWs by transducers with *different* orientations φ_{ex} from the range $41° < \varphi_{ex} < 47°$ and compare the observed diffraction patterns, we will see practically no differences, which is confirmed by both experiments and calculations.

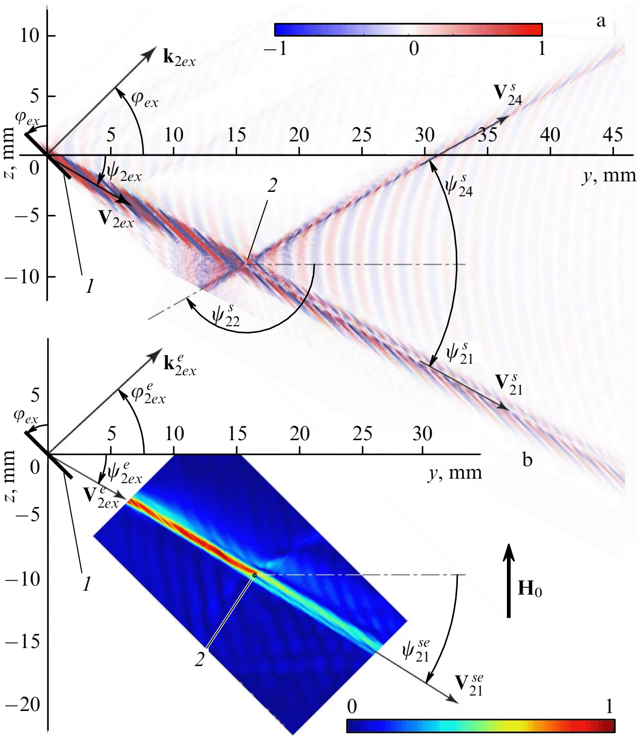

Figure 9. Calculated normalized distribution of the SW microwave magnetization (a) and experimental normalized distribution of the modulus $|A|$ of the complex amplitude (b) of an SW at frequency $f_2 = 3000$ MHz during its diffraction on a through-hole *2* of diameter $d = 250$ μm in a YIG film, for the case of SW excitation by a linear transducer *1* inclined to the vector $\mathbf{H}_0$ at an angle $\varphi_{ex} = 45°$.

Obviously, a similar situation occurs for SWs with *different* frequencies f in the range 2965 MHz $< f <$ 3010 MHz (i.e., frequencies close to $f_1 = 2970$ MHz), since at these frequencies there also exist wave propagation directions with quite small minimum values $\sigma^s \lesssim 0.1$ (below we will briefly refer to these directions as quasi-super-directional). That is, we will also not observe qualitative differences between the visualized patterns of SWs with *different* frequencies from the range 2965 MHz $< f <$ 3010 MHz — only the quasi-super-directional directions ψ^s will differ slightly for different frequencies (see Fig. 5), which is also evident from comparing Fig. 6a and Fig. 8a.

Thus, considering the above, the orientation of the excitation transducer (relative to vector $\mathbf{H}_0$) was set to $\varphi_{ex} = 45°$, which made it possible to effectively excite quasi-super-directional SW beams with $\sigma^s \lesssim 0.1$ over the frequency range 2965 MHz $\leqslant f \leqslant$ 3010 MHz.

As a result of measurements and processing of experimental data, a series of visualized patterns was obtained, describing the diffraction of a surface SW on the hole over the frequency range 2970 MHz $< f <$ 3100 MHz with a step of 5 MHz. It was found that the SW beam at frequency[16] $f_2 = 3000$ MHz was most accurately directed toward the center of the hole. Assuming that the transducer most efficiently excites SWs with a wave vector $\mathbf{k}_{21ex}$ normal to the transducer (i.e., with vector $\mathbf{k}_{21ex}$ oriented at angle $\varphi = \varphi_{21ex} = \varphi_{ex} = 45°$), we find that $k_{2ex}(\varphi_{ex}) = 79.19$ cm^{-1}, $\lambda_{2ex}(\varphi_{ex}) = 793$ μm and $\psi_{21ex}(\varphi_{ex}) = -32.27°$. The experimental pattern describing the distribution of the amplitude of an SW at frequency $f_2 = 3000$ MHz during its diffraction on a through-hole in the YIG film is presented in Fig. 9b, from which it is evident that the direction $\psi_{21ex}(\varphi_{ex}) = -32.27°$, corresponding to the excited quasi-super-directional SW beam, practically coincides with the direction $\psi^s_{21} = -32.1°$, which corresponds to the minimum value of σ^s in Fig. 5. As a result of the incidence of this beam on the hole, a distinct shadow in the form of a straight 'groove' is observed at a distance $L \approx 21$ mm (Fig. 9b).

Figure 9a shows the distribution of the microwave magnetization of the SW, calculated using the micromagnetic simulation technique and corresponding in all parameters to the experimental pattern in Fig. 9b.

As seen from comparing Figs 9a and 9b, the calculated and experimental diffraction patterns show good agreement: the performed calculations not only confirmed the experimental results but also demonstrated that the shadow from the hole can be observed at distances $L \sim 35$ mm from it!

Thus, it was discovered that as a result of diffraction on an hole of diameter $d = 250$ μm by a quasi-super-directional SW beam with $k_{2ex}(\varphi_{ex}) = 79.19$ cm^{-1} and wavelength $\lambda_{2ex}(\varphi_{ex}) = 793$ μm — which exceeds the hole diameter by $\lambda_{2ex}/d = 3.2$ times — a distinct shadow of width d arises in the direction $\psi^s_{21} \approx \psi_{21ex} = -32°$ begining from the hole, observed at a distance $L \approx 21$ mm (Fig. 9b), with the distance L exceeding the hole diameter by $L/d \approx 84$ times (in the calculations shown in Fig. 9a, the shadow is observed at $L \approx 35$ mm, and $L/d \approx 140$).

Furthermore, it is evident that when the original beam incident on the hole, there are arised the waves reflected from the hole (Fig. 9a) and characterized by all possible wave vectors (i.e., wave vectors whose orientations lie in the plane of the ferrite slab between the cutoff angles). Since $\lambda_{2ex}/d = 3.2$ and most directions corresponding to these secondary reflected waves are characterized by large diffraction divergence σ (see Fig. 5), the reflection is practically unobservable. The exceptions are only the directions ψ^s_{21}, ψ^s_{22}, ψ^s_{23} and ψ^s_{24}, corresponding to group velocity vectors $\mathbf{V}^s_{21}$, $\mathbf{V}^s_{22}$, $\mathbf{V}^s_{23}$ and $\mathbf{V}^s_{24}$, in which quasi-super-directional propagation of the reflected waves occurs (Fig. 9). The energy of these waves localizes along the four listed directions, which are shown in Fig. 9a. We note that all four quasi-super-directional beams are clearly visible only in Fig. 9a, which presents the calculations, because the pattern of high-frequency magnetization distribution is averaged over the thickness of the YIG film. In Fig. 9b, obtained by the probing method from the upper surface of the ferrite, the beams propagating along vectors $\mathbf{V}^s_{22}$ and $\mathbf{V}^s_{23}$ are practically invisible, since their energy is localized near the film surface adjacent to the substrate. At the same time, Fig. 9b shows some energy reflection in the direction of vector $\mathbf{V}^s_{24}$.

It should be noted that earlier, in Ref. [19], the diffraction of a surface SW on an hole in a YIG film was studied using the BLS method. No observation of shadows behind the hole was reported in that work (although very low-contrast shadows can be discerned in Figs 2 and 4 of Ref. [19]), and the diffraction beams arising behind the hole were characterized by the authors as 'caustic beams' or 'semicaustic beams.' Analyzing Ref. [19], we suppose that results similar to those described in Sections 5 and 6 could not be obtained there for several reasons: (1) the film dimensions were small (3×3 mm^2), and the wave distribution was measured for a very small area (0.8×0.8 mm^2); (2) the hole in the film had a diameter of 50 μm and was not a through-hole, and the film itself was thin (4.5 μm), which led to rapid attenuation of the wave amplitude as it propagated; (3) diffraction beams behind the hole were observed at a distance $L < 0.7$ mm, i.e., a situation where $L \sim \lambda$ prevailed; (4) the angular width of the SW diffraction beams and shadows behind the hole was neither measured, calculated, nor compared with the value λ/D; (5) the SW distribution in the film plane was measured at arbitrary frequencies (the work does not explain how these frequencies were chosen), whereas to observe the superresolution effect it was necessary to carry out measurements at a frequency at which the isofrequency dependence has inflection points.[17] Despite the critical comments made, we consider the results of Ref. [19] to be important, as this work is apparently the first study devoted to the diffraction of surface SW on a hole.

7. Postscript on the results of experiments and numerical calculations

After reading the preceding six sections, readers may remark that we have obtained interesting experimental and computational results that show good agreement — but it remains unclear why the superresolution effect arises. One would naturally desire a simple and intuitive physical explanation, as they say, 'in plain terms!'

We, of course, mind here that the diffraction of SWs by a circular hole, especially along an arbitrary direction in an anisotropic medium (described by a second-rank tensor!), is a mathematically complex problem. However, we also would not like this work to remain in the memory of readers as a simple description of some enigmatic phenomenon that cannot be explained simply and clearly.

With this in mind, below we will attempt not only to explain the physical essence of the phenomena under study in straightforward terms but also to demonstrate how a similar effect could be realized in other anisotropic media.

As is well known, any diffraction problem under rigorous analysis must be reduced to solving the corresponding wave equations with physically justified boundary conditions. However, exact diffraction theory (even for the simplest cases of wave diffraction in isotropic media) presents a highly complex mathematical challenge. Therefore, in many diffraction problems of practical interest, approximate estimates and methods are still widely used (e.g., estimates based on the

[16] Under this excitation geometry, SW beams at different frequencies will exhibit slightly different orientations ψ of the group velocity vector $\mathbf{V}$. As seen in Fig. 9, for the beam to hit the hole precisely, the corresponding ψ and φ values must be known with high accuracy. Some reasons why the beam at frequency $f_2 = 3000$ MHz was directed exactly at the hole, rather than the beam at $f_1 = 2970$ MHz, are discussed in Section 9.

[17] Apparently, the authors of Ref. [19] didn't know about the results of Ref. [8], assuming that such frequency does not exist for the surface SW.

Rayleigh resolution criterion or the method based on the Huygens–Fresnel principle involving the construction of Fresnel zones to describe diffraction in parallel beams). As for the study of diffraction problems for waves in anisotropic media, they are still in the initial stage of development and have scarcely been performed even for the simplest cases.

Based on this, we will use all currently available knowledge to make approximate estimates and, at least qualitatively, explain the phenomenon described above — the formation of a distinct shadow from an point-like object as a result of the diffraction of surface SW beams upon it for the geometries shown in Figs 6–9. In particular, we will attempt to carry out approximate calculations for the studied diffraction phenomena based on the Rayleigh resolution criterion.

8. Analysis of diffraction patterns based on Babinet's principle and the resolution criterion

As is well known, J.W. Rayleigh proposed the resolution criterion for two light sources in 1879. Subsequent studies of diffraction phenomena have shown that the Rayleigh criterion can be conveniently used not only to estimate the resolvability of two sources of light or other types of waves, but also for approximate calculations in a number of diffraction problems, e.g., for estimating the angular beam width or the resolving power of various optical instruments (or the human eye). In particular, formula (3), presented in Section 4 and derived in Ref. [8], corresponds to the Rayleigh resolution criterion applied to waves in anisotropic media for estimating the angular width $\Delta\psi$ of a SW beam or any other wave beam for which the medium is anisotropic. Substituting expression (5) into (3), we find that the angular beam width $\Delta\psi$ of any wave at a given frequency f in any anisotropic medium is given by the relation

$$\Delta\psi = \sigma\,\frac{\lambda}{D}\,, \tag{6}$$

where D is the exciter size (slit, antenna, excitation transducer), $\lambda = 2\pi/k$ is the wavelength, and σ is the relative angular beam width (whose physical meaning is explained in Section 4), which determines the wave's diffraction divergence. Obviously, in an anisotropic medium, the quantities λ and σ depend on the spatial direction (see Fig. 5) in accordance with the wave's dispersion relation. For waves in isotropic media, λ is a fixed quantity (at a given frequency f), $\sigma \equiv 1$ (see Section 4 and Fig. 5), and expression (6) transforms to the well-known Rayleigh criterion (4), which is commonly used to estimate the angular beam width in isotropic media.

Thus, the resolution criterion[18] (6) will allow us to estimate the angular width of SW beams in various problems. The remaining question is how to estimate the angular width of the shadows form the hole.

As is well known, diffraction theory includes Babinet's principle (see, e.g., [60]), which establishes a interdependence between the diffraction fields and patterns produced by complementary objects. Examples of such objects are, for instance, a thread and an opaque screen with a long slit (provided the thread thickness equals the slit width), or an opaque disk and an opaque screen with a circular hole of the same radius. Babinet's principle states that in such cases, the results of a diffraction calculation for one of these objects can

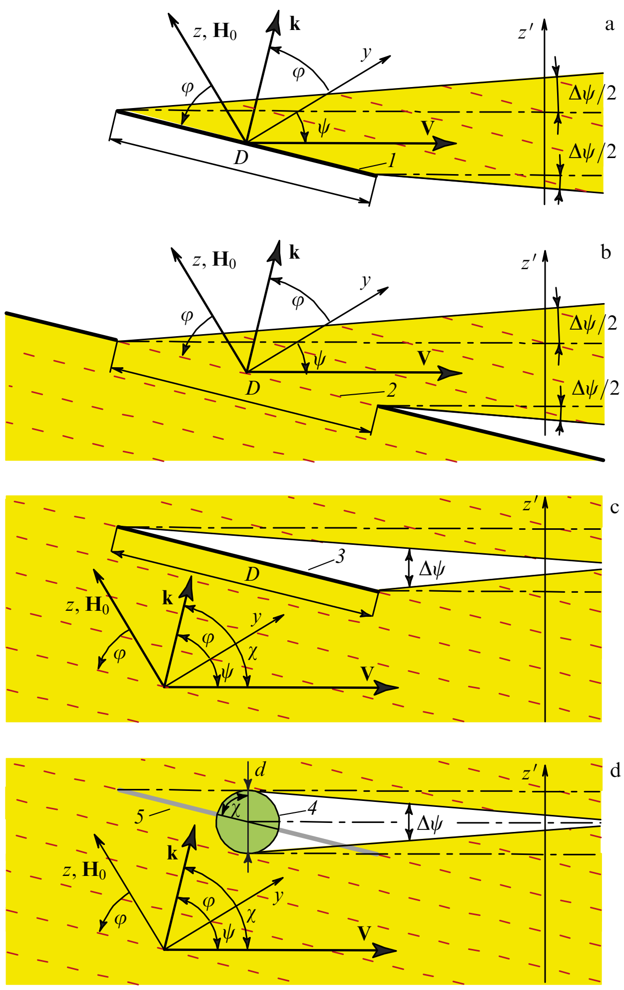

Figure 10. Simplified representation of SW diffraction patterns on various objects: excitation of an SW wave beam by a linear transducer *1* of length D (a); incidence of a plane SW on a slit *2* of length D in an opaque screen (b); incidence of a plane SW on an opaque screen *3* of length D (c); incidence of a plane SW on a circular hole *4* of diameter d in a ferrite film, where the diameter d is related to the length $D_{\rm im}$ of an imaginary transducer *5* by the relation $d = D_{\rm im}\cos\chi$ (d). The patterns are shown for the case where the SW wave vector $\mathbf{k}$ is normal to the object line (transducer, slit, or screen), and the z'-axis, along which real or imaginary measurements are performed, is perpendicular to the SW group velocity vector $\mathbf{V}$. Dashed lines correspond to the SW wave fronts.

be applied to the analogous diffraction problem for the complementary object. Below, we will assume that Babinet's principle is also valid in anisotropic media for analogous diffraction problems involving complementary objects.

To apply Babinet's principle for identifying analogous and complementary objects in the wave diffraction geometries under study, Fig. 10 presents simplified representations of certain diffraction patterns (corresponding to the diffraction geometries in Fig. 9). By analyzing these patterns we will be able to establish *analogs and complementary objects* for estimating the angular width of the shadow from the hole.

As seen by comparing Figs 10a and 10b, a linear SW excitation transducer of length D is physically analogous to an SW-exciting slit of length D in a thin, SW-impermeable screen [8]. However, this *analogy* is valid only for the case where the wave vector $\mathbf{k}_0$ of the SW incident on the slit is oriented normal to the slit line, and only if the following two conditions are simultaneously satisfied at the SW frequency f [8]: first, the transducer length must be much greater than the

[18] Of course, expression (3) can also be used as a resolution criterion.

SW wavelength, $D/\lambda_0 \gg 1$; second, the transducer length must be much smaller than the electromagnetic wavelength at the corresponding frequency, $D/\lambda_{\rm EMW} \ll 1$, since only in this case can the entire transducer aperture be considered in-phase, and the wave vector $\mathbf{k}_0$ of the excited SW can be considered normal to the transducer line. It is easy to see that in the microwave range, where $\lambda_{\rm EMW} \sim 3-30$ cm and $\lambda_0 \sim 0.05 - 1$ mm, both conditions can almost always be satisfied by choosing $D \sim 3-10$ mm.

Let us now determine the object that is *complementary* to a slit of length D in an opaque screen. Obviously, according to Babinet's principle, an opaque screen of length D, parallel to the slit line, will be such an object (Fig. 10c), since it is in this case that the transparent parts of one object (the slit in Fig. 10b) exactly coincide with the opaque parts of the other (the screen in Fig. 10c). That is, for the problems under consideration, it can be assumed that the diffraction fields and patterns arising in the far field region as a result of the wave beam excitation by a slit in an opaque screen (Fig. 10b) and by a linear transducer (Fig. 10a), are *mutually complementary* to the diffraction fields and patterns arising as a result of the wave beam diffraction on an opaque screen whose length equals the slit and transducer length D (Fig. 10c).

Let us now ask: is there any *analogy* between the diffraction properties (with respect to SWs) of the opaque screen shown in Fig. 10c and the properties of the hole in a ferrite film shown in Fig. 10d? Obviously, SW reflection from an opaque screen will be much more directional than reflection from a circular hole in a ferrite film. However, since we are interested only in the *passage and diffraction* of waves on the objects shown in Figs 10c and 10d, it is clear that these objects can be considered *analogous*,[19] and the diffraction fields created by them — *equivalent*,[20] if the diameter of the hole d and the opaque screen length D are related by (see Figs 10c and 10d)

$$D = \frac{d}{\cos\chi}\,, \tag{7}$$

where $\chi = \varphi + \psi$, and φ and ψ are the orientations of the wave vector $\mathbf{k}$ and the group velocity vector $\mathbf{V}$ of the wave *forming* the shadow behind the hole (recall that for the diffraction cases in Figs 6–9, the super-directional or quasi-super-directional wave forms the shadow, not the incident wave!).

Thus, we can consider that a through-hole of diameter d in a ferrite film is *equivalent to an imaginary opaque screen* that is parallel to the wave fronts of the incident wave and covers the same region of the incident beam as the hole of diameter d. The length $D_{\rm im}$ of this imaginary screen, determined by expression (7), *should be used* in the resolution criterion (6) to find the angular width of the shadow from the hole for waves in anisotropic media. It should be noted that for waves with *collinear* orientation of vectors $\mathbf{k}$ and $\mathbf{V}$ (i.e., for waves analogous to those in isotropic media), when $\chi = \varphi = \psi = 0$, the established equivalence of these objects is preserved. In this case, from Eqn (7) we obtain the expression $D = d$, and consequently, for collinear waves — as for waves in isotropic media — only the visible size of the object must be used to estimate the angular width of a beam or shadow[21] on the basis of the resolution criterion.

Thus, taking into account relation (7), the resolution criterion (6) will now allow us to estimate both the angular width of SW beams and the angular width of shadows.

In accordance with the simplified representation of the studied geometries in Fig. 10, we will perform estimates under the following assumptions:

(1) We will assume that estimates based on the resolution criterion (6) are valid and reliable only for the case $\lambda \ll D$ or, at minimum, for the case where λ is several times smaller than D (since the Rayleigh criterion, the theory of Ref. [8], and formulas (3)–(6) are valid precisely for this case).

(2) We will consider the studied problems as two-dimensional, since we are not interested in the dependence of SW characteristics on the coordinate x normal to the film plane, or we will use SW characteristics averaged over the coordinate x.

(3) For each diffraction geometry, we will use a new coordinate system $\Sigma'\{y', z'\}$ in the film plane (see Fig. 10), where the z'-axis is perpendicular to the group velocity vector $\mathbf{V}$ of the incident wave (Figs 10b, 10c, 10d); and for the geometry in Fig. 10a, we will assume that vector $\mathbf{V}$ corresponds to vector $\mathbf{k}$ normal to the transducer line.

(4) Within the framework of the two-dimensional problem, we will assume that real or imaginal measurements are performed along lines parallel to the z'-axis, that make it possible, using probing or BRS methods, to obtain the distribution of the SW amplitude and estimate the angular width of the beam or shadow.

(5) For the sake of brevity, we will not make any differences when referring to similar calculated and measured quantities (see footnote 15). The reasons for these differences will be discussed in the next section.

To estimate the angular width of SW wave beams in Figs 6–9, we will use the value of the angle φ_{ex} at which the excitation transducer is oriented in the corresponding experiment and we will find the corresponding values of the other calculated quantities for this angle.

To estimate the angular width of shadows in Figs 6–9, we will proceed from the assumption that shadows arise in the direction of super-directional or quasi-super-directional SW propagation — that is, in the direction where the dependence $\sigma(\psi)$ possesses its minimum value $\sigma = \sigma_{\min} = \sigma^s$. Therefore, finding the angles φ^s and ψ^s at which $\sigma = \sigma^s$, we will match to them the corresponding values of the other calculated quantities, including the length of the imaginary transducer $D_{\rm im}$ determined by formula (7), and the maximum distance $L_{\max}$ (at which the shadow can still be observed), calculated by the formula

$$L_{\max} = \frac{d}{\Delta\psi}\,. \tag{8}$$

[19] The case where the transducer aperture cannot be considered in-phase should be associated with a geometry in which the wave vector $\mathbf{k}_0$ of the incident SW is inclined at a certain angle relative to the slit line [8].

[20] If edge effects are neglected.

[21] This statement may appear to contradict what was stated earlier: we previously said that a shadow always arises in the direction of super-directional wave propagation, but now it turns out that it can also arise in the direction of collinear wave propagation when $\chi = \varphi = \psi = 0$. This contradiction is only seeming: in anisotropic media, a shadow indeed always arises in the direction of super-directional wave propagation, but sometimes this direction coincides with the direction of collinear wave propagation! For instance, Ref. [61] established that such a case occurs, for example, for SWs in a metallized ferrite slab: super-directional wave propagation arises at $\chi = \varphi = \psi = 0$ (see curve *2* in Fig. 2 of [61]).

Let us now estimate on the basis of the resolution criterion (6) the angular width of the beam and the shadow, primarily for the geometry in Fig. 9, and list for convenience the main characteristics of the beam or shadow.

For the beam in Fig. 9: $f_2 = 3000$ MHz and $\varphi_{ex} = 45°$. Based on this, we obtain: $\sigma_{2ex} = 0.0697$; $k_{2ex} = 79.19$ cm^{-1}; $\lambda_{2ex} = 793$ μm, $\lambda_{2ex}/D = 0.159$; $\psi_{2ex} = -32.27°$; $\Delta\psi_{2ex} = 0.0111(0.633°)$. Estimates based on the resolution criterion (6) are reliable since $\lambda \gg D$, and they correspond to the angular beam width in Fig. 9.

For the shadow in Fig. 9 (as well as for the analogous shadow in Fig. 8): $f_2 = 3000$ MHz and $\sigma_{2\,\min} = 0.0568$. Based on this, we obtain: $\varphi^s_{21} = 42.6°$, $\psi^s_{21} = -32.1°$, $k^s_2 = 66.65$ cm^{-1}, $\lambda^s_2 = 0.943$ mm, $D_{\text{im}} = 0.947$ mm, $\Delta\psi^s_2 = 0.0565(3.24°)$, $L_{\max} = 4.42$ mm. In this case, since $\lambda \sim D_{\text{im}}$, the estimates exceed the limits of applicability of criterion (6) ($\lambda \ll D$). Nevertheless, Fig. 9 shows that both in the experiment and in the numerical calculations, a distinct shadow behind the hole is observed at distances $L \sim 21$ mm and $L \sim 35$ mm, respectively.

Obviously, when estimating the angular width of the two shadows in Figs 6 and 7 (for $f_1 = 2970$ MHz), which correspond to angles $\varphi^s_{11.14} = \pm 44.6°$ and $\psi^s_{11.14} = \mp 31.1°$, we obtain from (6) $\Delta\psi^s_1 \sim 0$ and $L_{\max} \to \infty$, since $\sigma^s_1 \sim 0$. We note, however, that in this case, since $\lambda \sim D_{\text{im}}(\lambda^s_1 = 1.385$ mm and $D_{\text{im}} = 1.012$ mm), the estimates exceed the limits of applicability of criterion (6) ($\lambda \ll D$). Obviously, if $\sigma = 0$ is substituted into expression (6), then regardless of the ratio λ^s_1/D, one always obtains $\Delta\psi = 0$. Nevertheless, both in the experiment and in numerical calculations, two distinct shadows of width d are observed behind the aperture at a distance $\sim L = 21$ mm.

Estimating the angular width of the wave beams (for $f_1 = 2970$ MHz and $f_2 = 3000$ MHz at $\varphi_{ex} = 0$) in Figs 6–8, we obtain $\lambda_{1ex} = 4.012$ mm, $\sigma_{1ex} = 1.63$ and $\lambda_{2ex} = 2.476$ mm, $\sigma_{2ex} = 1.68$, and the angular width of both beams is very large: $\Delta\psi_{1ex} = 1.308(74.9°)$ and $\Delta\psi_{2ex} = 0.832(47.6°)$, so they can hardly be referred to as beams at all. Obviously, since $\lambda_{1ex} \sim D$ and $\lambda_{2ex} \sim D$ ($D = 5$ mm), the performed estimates exceed the limits of applicability of criterion (6) ($\lambda \ll D$), although they confirm the extremely strong diffraction divergence of these wave beams.

Summarizing the performed estimates, we can state the following.

Due to the presence of super-directional and quasi-super-directional wave propagation directions in the ferrite film, a new physical phenomenon arises in these directions: super-resolution. This phenomenon consists in the fact that a distinct shadow from a small (point-like) object (hole) exists at a significant distance from the object, and the observed angular resolution of the object (angular width) is many times smaller than the similar resolution obtained on the basis of Rayleigh resolution criterion (4).

The observation of this new phenomenon is confirmed both experimentally and through numerical and analytical calculations. Moreover, a similar phenomenon was recently observed by us during the study of backward volume SW diffraction on an through hole in a ferrite film [48].

Continuing the discussion of the obtained results, we note that readers may ask: why, in anisotropic media where super-directional wave propagation exists, a shadow arises from an object smaller than the wavelength, and why this shadow always appears in the direction (or directions) of super-directional propagation? As it is known, in isotropic media, a shadow from such an object does not arise!

To answer this question, let us first recall that the radiation pattern $F_{\text{isotr}}(\psi)$ of an elementary radiating element (in the equatorial plane) placed in an isotropic medium has a form of circle (see, e.g., Fig. 2.14 in [62]). In accordance with the developed concepts, the form of this pattern can be interpreted as a result of the *equivalence* of all directions of the isotropic medium with respect to diffraction — they all correspond to the *same* diffraction divergence, so $F_{\text{isotr}}(\psi) = \sigma(\psi) \equiv 1$ (see Fig. 5). In an anisotropic medium, however, different spatial directions are *not equivalent* with respect to diffraction, and if an elementary radiating element is placed in any anisotropic medium, its radiation pattern $F_{\text{anis}}(\psi)$ (in the far-field region of the equatorial plane) will obviously not be a circle. A rigorous electrodynamic calculation of such patterns [22] is beyond the scope of this work; however, it can be assumed that the pattern $F_{\text{anis}}(\psi)$ will resemble the dependence $1/\sigma(\psi)$ and will have maxima in directions corresponding to the minimum values of σ, since the radiated energy, redistributed significantly, will ultimately localize near these directions. [23] This fact is also confirmed by the diffraction patterns [24] presented in Figs 6–9. It is currently difficult to judge how narrow and directional the maxima of the pattern $F_{\text{anis}}(\psi)$ can be for a medium in which super-directional wave propagation is possible. Here, we only wish to emphasize that in an isotropic medium we have an *omnidirectional* elementary emitter, whereas in an anisotropic medium we have a *directional* one.

Let us now return to answering the original question. Suppose a wave front with wavelength λ, excited far from a small wave-opaque object of diameter d, reaches the object. According to Huygens' principle, the wave front reaching the object can be associated with a line of secondary wave sources and no such secondary sources present over a short segment of length d. If this situation occurs in an isotropic medium characterized by *omnidirectional* secondary elementary radiating elements, then for $d \ll \lambda$ and even for $d < \lambda$, the slight wavefront distortion arising behind the object quickly disappears as the wave propagates further and will be practically unnoticeable already at distances $d \sim \lambda$. If, however, this occurs in an anisotropic medium characterized by *directional* secondary radiating elements, then the slight wavefront distortion arising behind the object does not disappear quickly as the wave propagates further, even if $d \ll \lambda$, and can be observed at a significant distance L from the object. This is because the directional secondary radiating elements transfer energy predominantly in the direction with the minimum value of σ (or in the direction of super-

[22] A rigorous calculation of such patterns can presumably be performed using the methods employed in Ref. [62].

[23] As can be seen, this conclusion essentially agrees with the following conclusion made earlier in Ref. [18]: backward SW magnons focus along the normals to the inflection points of the wave's isofrequency dependence. However, both conclusions were derived from calculations based on different theoretical frameworks.

[24] It should be noted here that the diffraction patterns in Figs 6–9 are obtained for the meridional plane, in which an elementary radiating element placed in an isotropic medium has a figure-eight radiation pattern (see Fig. 2.14 in [62]) $F_{\text{isotr}}(\psi) = |\sin\psi|$ (when angles are measured from the normal to the radiating element axis). Obviously, for an elementary radiating element placed in an anisotropic medium, the analogous pattern $F_{\text{anis}}(\psi)$ will resemble $|\sin\psi|$ modulated by a dependence of the form $\sim 1/\sigma(\psi)$. Moreover, for angles ψ deviating from the normal to the emitter axis by no more than $\sim \pm 40°$ (i.e., lying within the cutoff angle interval), it is the factor $\sim 1/\sigma(\psi)$ *that will determine the pattern's shape* (just as for the equatorial plane patterns).

directional propagation, if it exists), thereby forming a shadow! Obviously, the maximum value of L will depend on the ratio between the object size d and the angular width of the radiation pattern of the elementary radiating element $\Delta\psi_F$ which fully corresponds to formula (8) and criterion (6). In this regard, we also note that the profile and direction of the shadow in Figs 5–8 will *not depend on the dimensions and orientation of the excitation transducers*:[25] if at least some amount of energy reaches the wave-opaque object (in this case, the hole), a distinct shadow will arise!

There is another important question that must be discussed in this work. Analyzing the resolution criterion (6), readers may ask: since the angular width of an SW beam $\Delta\psi$ can be zero (if $\sigma = 0$ is substituted into (6)), it follows that such a phenomenon as hyperresolution can exist, when an absolutely nonbroadening beam (or shadow) would be observed at an infinitely large distance from the exciter (or object)? This question is entirely reasonable, especially since Fig. 6a presents a geometry in which nonbroadening shadows oriented along the direction $\sigma_1^s \sim 0$ were observed. Indeed, in Fig. 6, we observe no tendency for the shadow from the hole to broaden up to a distance of $L \approx 21$ mm; the shadow simply gradually disappears due to wave attenuation itself (unfortunately, due to the presence of losses, SWs cannot propagate over very long distances).

Obviously, a comprehensive answer to this question requires calculating the radiation patterns $F_{\text{anis}}(\psi)$ discussed above. However, we would like to recall here some results that are already known. In particular, in earlier studies [8, 10] there was calculated the amplitude distribution A of the total magnetic potential of an SW excited by a slit of length D in an opaque screen as a function of angle ψ (see Figs 5, 6 in [8] and Fig. 3 in [10]) for various geometries (for the case $D \gg \lambda$), and the angular width of the resulting beam was determined from the $A(\psi)$ dependence. These works demonstrated that the $A(\psi)$ dependence is described by a function of the form $\sin\Phi/\Phi$; however, the value $\sin\Phi$ depends on the wave parameters in a more complex way than in isotropic media. Consequently, the $A(\psi)$ dependence resembles a $\sin\Phi/\Phi$ function that is strongly 'stretched' for certain values of ψ and strongly 'compressed' for others. It might seem that since the $A(\psi)$ dependence always possesses a central lobe, this lobe must always have some finite angular width $\Delta\psi$, and thus, the situation where $\Delta\psi = 0$ is impossible. It should be noted, however, that for a geometry in which an ideal super-directional beam is excited,[26] the $A(\psi)$ dependence in the far field region has a central lobe resembling a delta function: it has a maximum equal to 1 but *no angular width*, since the values of two zeros adjacent to the main maximum of the $A(\psi)$ dependence tend to each other! At the same time, such a beam naturally possesses a finite *absolute width*, which is determined by the exciter dimensions and is maintained during propagation!

Let us discuss the formulated question in an even more simplified way, focusing on the physical essence of the phenomena under study. As noted above, the relative angular beam width σ, which characterizes diffraction divergence in accordance with formula (5) can be equal to zero in certain directions ψ (see curve *1* in Fig. 5), in which super-directional propagation of the wave beam occurs. Let us logically consider what does zero diffraction divergence or super-directional wave propagation physically mean? In fact, this means the absence of diffraction for the wave beam propagating in that direction! And what does the absence of diffraction mean? It means that the laws of geometric optics can be applied in that direction! Thus, in anisotropic media, wave processes can be described within the framework of geometric optics when the value $\sigma = 0$ corresponds to the wave propagating in a given direction. However, as is well known, within geometric optics, a beam and a shadow cast by an object do not broaden and can be observed at infinitely large distances. Therefore, purely theoretically, a phenomenon such as hyperresolution could exist, where an absolutely nonbroadening beam (or shadow) would be observed at an infinitely large distance from the exciter (or object). Perhaps future studies on wave propagation in anisotropic media will show that the existence of this phenomenon is limited by certain distances or physical factors (e.g., due to losses) — this remains unknown at present, since research on wave diffraction in anisotropic media has only just begun, and the main results have been obtained only for SWs, which, incidentally, due to super-directional propagation, have been observed at record distances from the exciter of ~ 5 cm!

Unfortunately, we must conclude the discussion here. Although many interesting questions remain, answering them requires further research on wave diffraction, including research in other anisotropic media. Moreover, as will be evident from the material presented in the next section, even for SWs there are still unresolved problems. In particular, it turns out that it is not so easy to find out whether a super-directional beam or a quasi-super-directional beam (with a small value $\sigma \ll 1$) has been excited.

9. Reasons caused to slight differences between experimental and calculated results

As noted in Section 3, the parameters of the used YIG film were determined on the basis of approximation of the measured SW dispersion relation by the corresponding dispersion relation calculated in magnetostatic approximation. During the approximation process, the film thickness[27] and the effective saturation magnetization[28] of the YIG film were used as variable parameters, and the criterion for the best agreement between the measured and calculated relations was the minimum root-mean-square deviation of the dispersion curves. The measurement of the surface SW dispersion relation was performed for the case where the excitation transducer was parallel to the vector $\mathbf{H}_0$ and most efficiently excited SWs with wave vectors $\mathbf{k}$ oriented at $\varphi = 0$. For a series of fixed frequency values f, a corresponding series of experimental values k_y^e was found, that is, the dependence

[25] This conclusion can also be reached by analyzing the SW distribution patterns presented in Figs 2 and 4 of Ref. [19], although the emergence of shadows is not discussed in that work.

[26] Recall that in such a geometry, the wave vector of the incident wave falling on the slit is directed exactly toward the inflection point of the wave's isofrequency dependence, where $\partial\psi/\partial\varphi = 0$, and there is nothing mathematically unusual about this geometry.

[27] It might seem that the YIG film thickness could be measured, for example, using a microscope. However, a thickness measured by this way will include the thicknesses of the various oxide layers, which generally are presented on the YIG film surface and are not possessed by the properties of YIG. Therefore, a more accurate film thickness value can be found by the means of approximation.

[28] In reality, as a result of the approximation we find the difference M_{eff} between the value of $4\pi M_0$ and the uniaxial anisotropy field H_a (not the saturation magnetization $4\pi M_0$ — see Ref. [53] for details). For the sake of brevity, below we will refer to this difference M_{eff} as the effective magnetization.

$k_y^e(f, \varphi = 0)$ was actually measured and approximated. By approximating the experimental dependence $k_y^e(f, \varphi = 0)$ with the calculated dependence $k_y(f, \varphi = 0)$, one can ultimately find the values of thickness s and effective magnetization M_{eff}, which are usually considered as the actual parameters of the ferrite film.

However, if we measure the SW dispersion relation at a different angle φ (i.e., with an arbitrary orientation of the transducer) and then compare this dependence with the theoretically calculated for the found values s and M_{eff}, we will see that the agreement between the curves becomes worse than it was at $\varphi = 0$, and the larger the value of φ, the poorer the match. This mismatch naturally affects on the SW isofrequency dependences: if we compare the experimental and theoretical isofrequency dependences, the best agreement, as already noted, will be observed for the points where these dependences intersect the k_y axis (since the approximation was performed precisely for these points), while with increasing φ, the isofrequency dependences will differ more significantly. In other words, we would observe that the experimental and theoretical isofrequency dependences have slightly different asymptotes or cutoff angles corresponding to waves with $k \to \infty$. Obviously, because of this reason the calculated and experimental wave vectors $\mathbf{k}$ and $\mathbf{k}^e$, directed at the same angle φ, will have different magnitudes, and the corresponding calculated and experimental group velocity vectors $\mathbf{V}$ and $\mathbf{V}^e$ will differ slightly in both magnitude and orientation ψ and ψ^e (that is why the notations of these values differ in Fig. 9).

The reason for the observed differences between the experimental and calculated SW characteristics is a certain imperfection of the used methodologies. Unfortunately, at present, there is no methodology that would allow simultaneous approximation of the entire experimental SW dispersion surface $f(k_y^e, k_z^e)$ (or $f(k^e, \varphi^e)$) and that would provide the coincidence of the cutoff angle values too. Presumably, when developing such a methodology, in addition to the uniaxial and cubic anisotropy fields accounted for in the methodologies of [52, 53], it will be necessary to use additional parameters describing the ferrite film and the SW. In this regard, it should be noted that the superresolution effect described above provides an excellent opportunity to measure with high precision the angles ψ^{se} that correspond to the inflection points of the isofrequency dependence and describe the directions of super-directional SW propagation (and these angles are much easier to measure than the cutoff angles corresponding to SWs with $k \to \infty$). The measuring of the angles ψ^{se} could serve as the basis for developing a new, more accurate methodology for determining ferrite film parameters.

There is another reason for the differences between the experimental and calculated values of the corresponding SW characteristics. The fact is that a real excitation transducer isn't a perfectly in-phase exciter: at frequencies of 2–3 GHz for a transducer length $D \sim 5$ mm, a phase shift $\Delta\theta$ of several degrees arises between its ends, as was previously noted in Ref. [11]. The presence of this phase shift $\Delta\theta$ causes the experimental wave vector $\mathbf{k}_{ex}^e$, corresponding to the most efficiently excited SW, to deviate slightly from the normal to the transducer line. Consequently, the angle φ_{ex}, which defines the transducer orientation, is not equal to the angle φ_{ex}^e, which defines the orientation of vector $\mathbf{k}_{ex}^e$ (that is why the notations of these values differ in Fig. 9). Moreover, it is difficult to find the shift $\Delta\theta(f) = \varphi_{ex} - \varphi_{ex}^e(f)$ in order to take it into account in the calculations.

We note that the presence of the phase shift $\Delta\theta$ can also be seen in the experimental diffraction patterns. Obviously, if $\Delta\theta$ was zero, the diffraction patterns in Figs 6a and 8a would be mirror-symmetric with respect to the y-axis. In reality, however, the patterns in Figs 6a and 8a are not strictly symmetric about the y-axis (this asymmetry is especially evident in the analogous pattern shown in Fig. 6 of Ref. [11]).

Unfortunately, since the value of $\Delta\theta$ is unknown, we cannot state with certainty whether the wave beam excited in our experiment had a value σ exactly equal to zero, or whether σ was only approximately zero.

Nevertheless, these small differences between the experimental and calculated SW characteristics do not affect the reability and validity of the superresolution effect, which is the subject of the study in this work.

10. Conclusion

The possibility of overcoming the diffraction limit in anisotropic media is discussed in this work. In order to solve this problem, we demonstrate for the first time the occurrence of a superresolution effect, in which a distinct, practically non-broadening shadow from a point-like object is observed at distances significantly (by 1–2 orders of magnitude) greater than the values predicted by the Rayleigh resolution criterion.

In particular, the diffraction of a surface spin wave with wavelength λ on a point-like object (a through-hole of diameter d in a ferrite film) is investigated experimentally and on the basis of numerical calculations for various excitation geometries using a linear transducer for the cases $\lambda/d = 3.2$ and $\lambda/d = 5.54$. It is found that for geometries in which the incident wave is quasi-super-directional (i.e., characterized by a relative angular beam width $\sigma \lesssim 0.1$ and has almost no diffraction divergence), wave diffraction on the hole gives rise to a new physical phenomenon — superresolution, in which a distinct shadow from the hole exists at a considerable distance $L \gg \lambda$, and the observed angular resolution d/L is many times smaller than the angular resolution observed for a similar geometry in isotropic media. It is also established that for geometries where the incident wave exhibits large diffraction divergence (characterized by $\sigma \gtrsim 1.5$), superresolution effects occur only if the wave's isofrequency dependence possesses either inflection points (for which $\sigma \sim 0$), corresponding to super-directional wave propagation or points with a minimum value of the isofrequency dependence curvature (for which $\sigma \lesssim 0.1$), corresponding to quasi-super-directional wave propagation. It is demonstrated that, regardless of the initial parameters of the incident spin wave and its excitation geometry, superresolution effects — distinct shadows formed by excited secondary waves behind the hole — always arise *exclusively* in the directions of super-directional and quasi-super-directional wave propagation (with $\sigma \lesssim 0.1$), and not arise in the direction of the incident wave.

Since the phenomena described above cannot be explained by the well-known Rayleigh resolution criterion, a new resolution criterion is formulated in this work. This new criterion takes into account the dependence of wave diffraction divergence on spatial propagation directions in anisotropic media.

The application of Babinet's principle (assuming its validity in anisotropic media) to the analysis of the studied diffraction patterns allowed us to identify both analogous and mutually complementary objects for the diffraction geometries under investigation. In particular, it was established that a linear transducer of length D used to excite SWs is analogous to a slit of length D in an opaque screen, provided the wave incident on the slit has a wave vector $\mathbf{k}_0$ oriented normal to the slit line. It was also found that the aforementioned slit and transducer are complementary to an opaque screen of length D parallel to them, while a hole in a ferrite film (when studying transmitted waves) is analogous to an opaque screen (parallel to the wave fronts of the incident wave) whose imaginary length $D_{\rm im}$ covers the same region of the incident beam as the hole of diameter d. The proposed resolution criterion, combined with the application of Babinet's principle, made it possible to carry out approximate calculations for all obtained diffraction patterns and provided a clear explanation for the occurrence of super-directional and superresolution effects.

The work also describes the reasons for the differences between the measured and calculated spin wave parameters. In particular, it is noted that one of these reasons is the absence of a methodology that would allow simultaneous approximation of the entire experimental SW dispersion surface and provide agreement not only between the calculated and measured dispersion relations but also between the SW isofrequency dependence. In this regard, it is proposed to use the superresolution effect to measure the angles of super-directional SW propagation (these angles can be measured with high accuracy) and use their values in the approximation. Another reason of the observed differences between the measured and calculated SW parameters is the outphasing of the excitation transducer, because of the wave vector of the most efficiently excited SW is always slightly deviated from the normal to the transducer line.

The results obtained in this work can be used to perform approximate calculations based on the formulated resolution criterion to search for geometries that could realize superresolution effects in other anisotropic media, such as ferrites, antiferromagnets, plasmas, the Earth's ionosphere, uniaxial optical and acoustic crystals, as well as various metamaterials. Furthermore, for practical applications, the use of the superresolution effect would likely enable the observation of objects whose dimensions are much smaller than the wavelength.

The authors are grateful to V.P. Ivanov for fabricating the aperture in the ferrite film, to A.Yu. Annenkov for assistance in preparing the measurements, and to A.B. Khutieva for help with the numerical calculations.

E.H. Lock and S.V. Gerus carried out the research presented in this work as part of the State Task of the V.A. Kotelnikov Institute of Radio Engineering and Electronics, Russian Academy of Sciences, while A.V. Sadovnikov conducted his work under the Russian Science Foundation (RSF) Project No. 23-29-30027 (investigation of spin wave propagation inside a ferrite with an inhomogeneous distribution of internal fields using micromagnetic simulation).

References

1. Heintzmann R, Gustafsson M G L *Nature Photon.* **3** 362 (2009)
2. Zhuang X *Nature Photon.* **3** 365 (2009)
3. Hell S W, Schmidt R, Egner A *Nature Photon.* **3** 381 (2009)
4. Pendry J B, Smith D R *Phys. Today* **57** (6) 37 (2004)
5. Eleftheriades G V, Balmain K G (Eds) *Negative-Refraction Metamaterials. Fundamental Principles and Applications* (New York: Wiley, IEEE Press, 2005) DOI:10.1002/0471744751
6. Veselago V G *Sov. Phys. Usp.* **10** 509 (1968); *Usp. Fiz. Nauk* **92** 517 (1967)
7. Lock E H *Phys. Usp.* **51** 375 (2008); *Usp. Fiz. Nauk* **178** 397 (2008)
8. Lock E H *Phys. Usp.* **55** 1239 (2012); *Usp. Fiz. Nauk* **182** 1327 (2012)
9. Lokk E G *J. Commun. Technol. Electron.* **60** 97 (2015); *Radiotekh. Elektron.* **60** 102 (2015)
10. Lock E H *Bull. Russ. Acad. Sci. Phys.* **81** 996 (2017); *Izv. Ross. Akad. Nauk. Ser. Fiz.* **81** 1104 (2017)
11. Annenkov A Yu, Gerus S V, Lock E H *Europhys. Lett.* **123** 44003 (2018)
12. Annenkov A Yu, Gerus S V, Lock E H *EPJ Web Conf.* **185** 02006 (2018)
13. Martyshkin A A et al. *Phys. Rev. Applied* **22** 014037 (2024)
14. Vashkovskii A V et al. *Radiotekh. Elektron.* **32** 2295 (1987)
15. Vashkovskii A V et al. *Radiotekh. Elektron.* **33** 876 (1988)
16. Vashkovskii A V, Stal'makhov A V, Shakhnazaryan D G *Sov. Phys. J.* **31** 908 (1988); *Izv. Vyssh. Uchebn. Zaved. Fiz.* (11) 67 (1988)
17. Vashkovskii A V, Stal'makhov V S, Sharaevskii Yu P *Magnitostaticheskie Volny v Elektronike Sverkhvysokikh Chastot* (Magnetostatic Waves in Ultra-High-Frequency Electronics) (Saratov: Izd. Saratov. Univ., 1993)
18. Veerakumar V, Camley R E *Phys. Rev. B* **74** 214401 (2006)
19. Gieniusz R et al. *Appl. Phys. Lett.* **102** 102409 (2013)
20. Pirro P et al. *Nature Rev. Mater.* **6** 1114 (2021)
21. Zhang Z et al. *Appl. Phys. Lett.* **115** 232402 (2019)
22. Chumak A V et al. *IEEE Trans. Magn.* **58** 0800172 (2022)
23. Sebastian T et al. *Front. Phys.* **3** 35 (2015)
24. Nikitov S A et al. *Phys. Usp.* **63** 945 (2020); *Usp. Fiz. Nauk* **190** 1009 (2020)
25. Demidov V E et al. *Appl. Phys. Lett.* **105** 172410 (2014)
26. Nikitov S A, Filimonov Yu A *Radiotekh. Elektron.* **70** 292 (2025)
27. Davies C S et al. *Appl. Phys. Lett.* **107** 162401 (2015)
28. Shiota Y et al. *Appl. Phys. Lett.* **116** 192411 (2020)
29. Dudko G M et al. *Tech. Phys.* **67** 970 (2022); *Zh. Tekh. Fiz.* **92** 1151 (2022)
30. Makartsou U et al. *Appl. Phys. Lett.* **124** 192406 (2024)
31. Khutieva A B et al. *Bull. Russ. Acad. Sci. Phys.* **85** 1205 (2021); *Izv. Ross. Akad. Nauk. Ser. Fiz.* **85** 1542 (2021)
32. Swyt M S et al. *Appl. Phys. Lett.* **124** 112410 (2024)
33. Bloch F *Z. Phys.* **61** 206 (1930)
34. Akhiezer A I, Bar'yakhtar V G, Peletminskii S V *Spinovye Volny* (Moscow: Nauka, 1967); Translated into English: *Spin Waves* (Amsterdam: North-Holland Publ. Co., 1968)
35. Damon R W, Eshbach J R *J. Phys. Chem. Solids* **19** 308 (1961)
36. Gurevich A G, Melkov G A *Magnitnye Kolebaniya i Volny* (Moscow: Nauka, 1994); Translated into English: *Magnetization Oscillations and Waves* (Boca Raton, FL: CRC Press, 1996)
37. Lock E H, Gerus S V *Phys. Usp.* **67** 1257 (2024); *Usp. Fiz. Nauk* **194** 1330 (2024)
38. Vashkovskii A V et al. *Pis'ma Zh. Tekh. Fiz.* **12** 487 (1986)
39. Vlannes N P *J. Appl. Phys.* **61** 416 (1987)
40. Annenkov A Yu, Gerus S V *J. Commun. Technol. Electron.* **57** 519 (2012); *Radiotekh. Elektron.* **57** 572 (2012)
41. Borovik-Romanov A S, Kreines N M *Phys. Rep.* **81** 351 (1982)
42. Demidov V E et al. *Appl. Phys. Lett.* **90** 172508 (2007)
43. Demokritov S O, Demidov V E *IEEE Trans. Magn.* **44** 6 (2008)
44. Kruglyak V V, Demokritov S O, Grundler D *J. Phys. D* **43** 264001 (2010)
45. Sadovnikov A V et al. *Phys. Rev. B* **96** 144428 (2017)
46. Gubanov V A et al. *Phys. Rev. B* **107** 024427 (2023)
47. Bessonov V D et al. *Phys. Rev. B* **109** 024415 (2024)
48. Gerus S V et al. *Bull. Russ. Acad. Sci. Phys.* **86** 1361 (2022); *Izv. Ross. Akad. Nauk. Ser. Fiz.* **86** 1642 (2022)
49. Gerus S V, Annenkov A Yu, Lock E H *J. Magn. Magn. Mater.* **563** 169747 (2022)
50. Zubkov V I, Lokk E G, Shcheglov V I *Sov. J. Commun. Technol. Electron.* **35** (13) 66 (1990); *Radiotekh. Elektron.* **35** 1617 (1990)
51. Zubkov V I et al. *Zh. Tekh. Fiz.* **59** (12) 115 (1989)
52. Voronenko A V, Gerus S V, Krasnohzen L A *Mikroelektronika* **18** 61 (1989)
53. Vashkovskii A V, Lokk E G, Shcheglov V I *Phys. Solid State* **41** 1868 (1999); *Fiz. Tverd. Tela* **41** 2034 (1999)
54. Gerus S V, Lock E H, Annenkov A Yu *J. Commun. Technol. Electron.* **66** 1378 (2021); *Radiotekh. Elektron.* **66** 1216 (2021)
55. Khutieva A B, Sadovnikov A V, Certificate of state registration of a computer program, 2020666510, dated 10.12.2020
56. Demidov V E et al. *Phys. Rev. B* **77** 064406 (2008)
57. Prokhorov A M (Ed.-in-Chief) *Fizicheskaya Entsiklopediya* (Physical Encyclopedia) Vol. 3 (Moscow: Bol'shaya Rossiiskaya Entsiklopediya, 1992)
58. Prokhorov A M (Ed.-in-Chief) *Fizicheskaya Entsiklopediya* (Physical Encyclopedia) Vol. 2 (Moscow: Bol'shaya Rossiiskaya Entsiklopediya, 1992)
59. Crawford F S (Jr.) *Berkeley Physics Course* Vol. 3 *Waves* (New York: McGraw-Hill, 1968)
60. Born M, Wolf E *Osnovy Optiki* (Moscow: Nauka, 1970); Translated from English: *Principles of Optics* (Oxford: Pergamon Press, 1969)
61. Lock E H, Gerus S V *J. Commun. Technol. Electron.* **68** 971 (2023); *Radiotekh. Elektron.* **68** 884 (2023)
62. Markov G T, Petrov B M, Grudinskaya G P *Elektrodinamika i Rasprostranenie Radiovoln* (Electrodynamics and Radio Wave Propagation) (Moscow: Sovetskoe Radio, 1979)